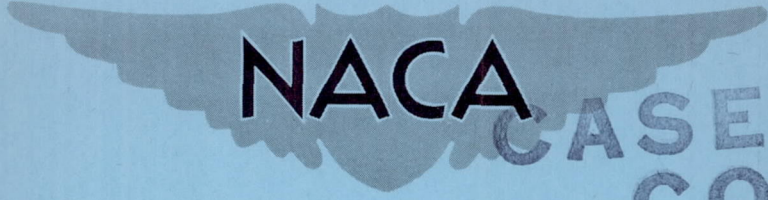


CONFIDENTIAL

NACA RM A54L13



CASE FILE COPY

RESEARCH MEMORANDUM

INITIAL EXPERIMENTS ON THE AERODYNAMIC COOLING
ASSOCIATED WITH LARGE-SCALE VORTICAL
MOTIONS IN SUPERSONIC FLOW

By A. J. Eggers, Jr., and C. A. Hermach

Ames Aeronautical Laboratory
Moffett Field, Calif.

CLASSIFICATION CHANGED TO UNCLASSIFIED
AUTHORITY: NASA PUBLICATION ANNOUNCEMENT NO. 4
EFFECTIVE DATE: FEBRUARY 10, 1959
WHL

CLASSIFIED DOCUMENT

This material contains information affecting the National Defense of the United States within the meaning of the espionage laws, Title 18, U.S.C., Secs. 793 and 794, the transmission or revelation of which in any manner to an unauthorized person is prohibited by law.

NATIONAL ADVISORY COMMITTEE FOR AERONAUTICS

WASHINGTON

March 8, 1955

CONFIDENTIAL

NATIONAL ADVISORY COMMITTEE FOR AERONAUTICS

RESEARCH MEMORANDUMINITIAL EXPERIMENTS ON THE AERODYNAMIC COOLING
ASSOCIATED WITH LARGE-SCALE VORTICAL
MOTIONS IN SUPERSONIC FLOW

By A. J. Eggers, Jr., and C. A. Hermach

SUMMARY

It is conjectured that convective heat transfer to a surface in supersonic flow may be reduced by periodically imposing a large-scale vortical motion on the boundary layer. The resulting vortex is expected to remove part of the heat convected to the surface by the normal boundary layer.

This conjecture was checked with experiments at Mach numbers from 3 to 5 on two bodies of revolution having spikes protruding from a blunt nose. The basic body was a truncated cone of fineness ratio 2. When pulsating flow occurred at the nose, turbulent masses of air were periodically discharged over the body with a large-scale vortical motion. Under these circumstances it was indicated that the average rate of heat transfer at zero angle of attack could be reduced by at least 22 percent. The recovery factors were reduced by as much as 25 percent. At small angles of attack the recovery factors were higher on the windward side than on the leeward side of a body. Although no measurements were made, it is anticipated from considerations of symmetry that the average rate of heat transfer varies only slightly about zero angle of attack.

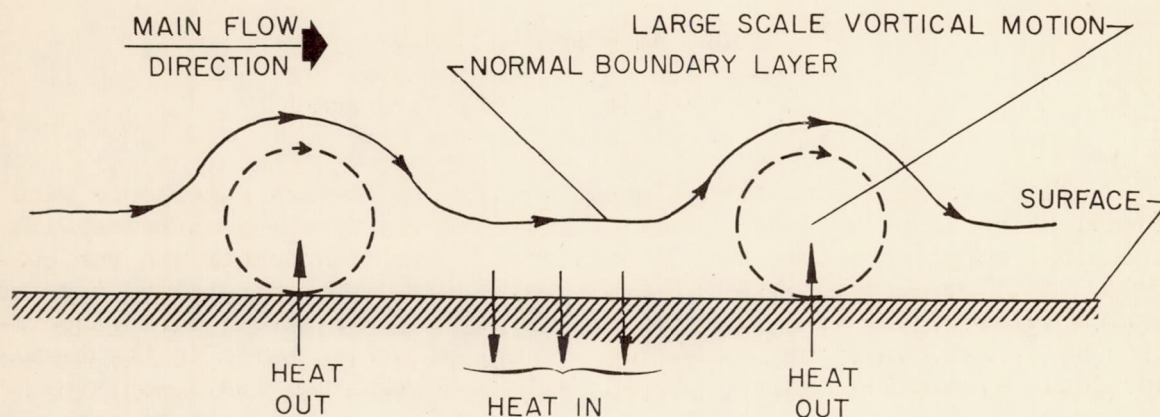
Drag was decreased by as much as 35 percent by protruding the spikes from the blunt-nose bodies at angles of attack up to 4° . On the other hand, lift was increased by as much as 100 percent, while pitching moment about the base was increased only slightly.

INTRODUCTORY REMARKS

Considerable effort is being devoted to reducing the aerodynamic heating of vehicles in supersonic flight. This effort has produced a number of promising ideas (see, e.g., refs. 1 through 5), all based on

the premise that flow bounding a surface will be either laminar, transitional, or turbulent, and more or less steady. The large bulk of experimental data do, to be sure, substantiate this premise. Nevertheless, it seems worthwhile to inquire if there can be a basically different flow which transfers less heat to a surface than the usual boundary layer. In this regard nonsteady flows may warrant attention.

Consider, in particular, the hypothetical flow shown on the sketch.



This flow differs from the normal boundary layer in one important respect - a large-scale vortical motion exists in the boundary layer at short intervals along the surface. By "large scale" it is meant that the diameter of each vortex is of the order of or greater than the thickness of the boundary layer. Now let us assume that these vortices are made up of air from the main flow and, further, that the surface over which they pass is at some reasonable temperature greater than ambient air temperature. It is argued then that part of the heat convected to the surface in the region of the normal boundary layer should be convected from the surface in the region of a vortex since the peripheral portion of the vortex should be cooler than the surface. That is to say, each large-scale vortex should create a negative temperature gradient at the surface and thus abstract heat therefrom. This boundary-layer-vortex combination offers promise, then, of convecting less heat to a surface than the normal boundary layer. The cooling by the vortices should, of course, depend upon both their size and spacing.

These considerations lead naturally to the questions of what shape might be employed to test this "boundary-layer-vortex" hypothesis, and how might the vortices be generated? The body of revolution was chosen for study because it constitutes a practical aerodynamic shape. It would be most desirable to generate the vortices at the nose of the body. In this regard, recent work of Beastall and Turner (ref. 6) has shown that a high-frequency pulsating flow is caused by a spike protruding in front of a bluff body at supersonic speeds. It was our thought that a large-scale

vortex might be discharged from the nose in concert with each pulsation, and further, that the resulting flow aft of the nose might resemble the boundary-layer-vortex flow. Accordingly, it was undertaken to investigate experimentally the heat transfer and aerodynamic characteristics of several bodies of revolution, including two with spike noses, in supersonic flow. The remainder of this paper is devoted to a description and discussion of this research (see the Appendix for a summary of the notation).

EXPERIMENT

Apparatus and Tests

All tests were conducted in the Ames 10- by 14-inch supersonic wind tunnel which is of the continuous-flow, nonreturn type and operates with a nominal supply pressure of 6 atmospheres. The Mach number was varied from 3 to 5 by changing the relative positions of the symmetrical top and bottom walls of the wind tunnel. The supply air was heated during operation at a Mach number of 5 in order to prevent condensation in the test section. A detailed description of the wind tunnel and its associated equipment, and of the characteristics of the flow in the test section may be found in reference 7.

The measured heat-transfer characteristics included both heat-transfer rates and recovery temperatures for the test models. Measured aerodynamic characteristics included lift, drag, and pitching moment. The tests were conducted at zero angle of attack over the Mach number range, and at angles of attack up to 4° at a Mach number of 3.5. All models were sting supported from the rear, and angle of attack was obtained by inclining the support system (see ref. 7).

Wind-tunnel-calibration data were employed in combination with measured stagnation pressures to obtain the stream static and dynamic pressures of the tests. Reynolds numbers based on the maximum diameter of the models were

| <u>Mach number</u> | <u>Reynolds number, million</u> |
|--------------------|-------------------------------------|
| 3.00 | 1.57 |
| 3.50 | 1.90 |
| 4.23 | 1.44 |
| 5.05 | 0.70 |

Models and Instrumentation

The shapes tested during this investigation are shown in figure 1. They are all bodies of revolution of fineness ratio 2 (exclusive of spike-nose assembly); hence, they are perhaps most representative of the forward portion of a complete body. It is important to keep in mind, however, that they also represent possible ballistic vehicles (see, e.g., ref. 5) or projectiles. The truncated cone is the basic body from which the two spike-nose configurations were derived. The conical spikes were chosen after studying the work of Beastall and Turner (ref. 6), the principal aim being to obtain pulsating flow with spikes of practical proportions. The semicircular cutout was tested in the anticipation that it would improve vortex generation. All models had a base diameter of 2 inches and a basic length of 4 inches. The truncated cone (basic body) had a nose diameter of 1.333 inches (i.e., two thirds of the base diameter). The conical spikes had a total included angle of 15° . Separate models were built to determine recovery temperatures, total heat transfer, afterbody heat transfer, and aerodynamic forces and moments.

A typical recovery-temperature installation, with details of the geometry of the spike and the semicircular cutout, is shown in figure 2. The recovery-temperature models were constructed of stainless steel and had a wall thickness on the afterbody of 0.025 inch. Iron-constantan thermocouples were imbedded in the wall to determine local recovery temperatures at various positions on the surface. The points of support for the thin wall were insulated with nylon bushings to reduce direct heat transfer between the wall and the sting support.¹ The two spike-nose models were equipped with movable spikes to permit their extension and retraction during testing.

Typical model installations for the determination of total heat transfer and afterbody heat transfer are shown in figures 3 and 4. The heat-transfer models were made of Duralumin and were of heavy construction to minimize temperature differentials within the models. The spike-nose configurations had changeable fixed-length spikes. An electric heater was used to raise the model temperature to various values above recovery temperature. This model heater was connected to a thin-walled cylinder

¹It should be noted that on the model with the semicircular cutout there was metal-to-metal contact between the nose piece and the thin-walled afterbody. In order to determine the effect on temperatures of the heat transfer through this section, experiments were conducted with a 0.005-inch air gap in place of the contact. It was found that although contact substantially increased the temperature indicated at the first thermocouple ($X = .31$ inch) on the afterbody, it did not appreciably affect the temperatures farther downstream. All experiments with this configuration were conducted with metal-to-metal contact; hence, the first thermocouple readings were dependent on the degree of this contact which was not, of course, always the same.

which constituted the support sting near the model base. A guard heater was installed on the cylinder a short distance aft of the model heater. The power to the guard heater was adjusted so that no temperature differential existed between the guard heater and the model heater. In this manner heat losses from the model heater to the model support structure were essentially eliminated. Accordingly, the electrical power required by the model heater to maintain a given model temperature determined the rate of heat transfer from the model to the air.

The power supplied to the model was determined by measuring the resistance of the model heater and the voltage across the heater. The heater resistance was essentially independent of temperature. Model temperatures were measured in the region of the model heater using iron-constantan thermocouples. Differential thermocouples were used to indicate when zero temperature differential occurred between the two heaters.

The models used to obtain aerodynamic characteristics were made of steel - again the spike-nose configurations had changeable fixed-length spikes. Lift, drag, and pitching moment were measured with a conventional strain-gage balance housed in a boom aft of the model. Tare forces on the sting support were essentially eliminated by a 5/8-inch-diameter shroud. Base pressures were measured to determine the lift and drag contributed by the base force.

Flow about the test models was photographed with a shadowgraph apparatus employing a high-speed-spark light source. Spark time durations of 1/4 microsecond or less were used in order to effectively "stop" the high-frequency pulses associated with the spike-nose configurations.

Accuracy of Test Results

The errors which influence the test results in general are as follows: Errors in angle-of-attack values are due mainly to uncertainties in corrections for stream angle and for deflections of the model support system. These errors are estimated not to exceed $\pm 0.2^\circ$. Errors in spike extension for the spike-nose configurations did not exceed ± 0.005 inch. Mach number in the region of the test section where the models were located did not vary more than ± 0.02 from the mean values. The Reynolds number for a given Mach number did not differ by more than $\pm 10,000$ from the mean values.

The maximum error in local recovery-temperature measurements due to instrument error is approximately $\pm 1^\circ$ R. The corresponding error in recovery factor is approximately ± 0.005 . The additional error due to heat transfer through a model is, for the most part, less than this amount.

The heat-transfer rates are in error due to uncertainties in measurements of heater resistance, heater voltage, and differential temperature between the heaters. This error does not exceed ± 2 percent. The heat-transfer coefficients are in error for the same reasons, and further, they depend on the difference between the measured recovery temperature of a model and the measured temperature of the model with heat flow to the air. The maximum error in measured temperature was constant at approximately $\pm 0.25^\circ \text{R}$;² accordingly, the possible error in heat-transfer coefficient varies as a function of the measured temperature difference. For example, the error in heat-transfer coefficient for a 10°R temperature differential could be as high as $\pm 0.0003 \text{ Btu/sq ft, sec, }^\circ \text{R}$, while for a temperature differential of 30°R , it should not exceed $\pm 0.0002 \text{ Btu/sq ft, sec, }^\circ \text{R}$.

The errors in the force and moment results were due primarily to uncertainties in the measurements of these quantities by the balance system and uncertainties in the determination of free-stream dynamic pressures and base pressures. These uncertainties result in maximum possible errors in lift, drag, and pitching-moment coefficients of ± 0.002 .

Summarizing, the recovery factors are estimated to be accurate within ± 0.005 , the heat-transfer coefficients within $\pm 0.0002 \text{ Btu/sq ft, sec, }^\circ \text{R}$, and the lift, drag, and pitching-moment coefficients within ± 0.002 . It should be emphasized that all the above discussion concerns maximum errors and that, for the most part, the results presented are in error by less than half of the estimates.

RESULTS AND DISCUSSION

Pulsating Flow Phenomena

It was undertaken at the outset of this experimental work to determine the range of spike extension over which pulsating flow occurred. It was observed optically that pulsations began when a spike first pierced the detached shock wave ($\bar{X} = 0.4$ inch at $\alpha = 0^\circ$, $M_0 = 3.5$). Pulsations continued and with increasing amplitude (i.e., fore-and-aft shock motion) until a spike extension was reached ($\bar{X} = 2$ inches) which, rather abruptly, produced a quasi-steady separated flow from the tip of the spike. This quasi-steady-type flow was maintained with further spike extension. These results are in agreement with those obtained by Beastall and Turner with spike-nose models.

In order to obtain additional information on the pulsating flow phenomena, a series of shadowgraph pictures (spark source) were taken at

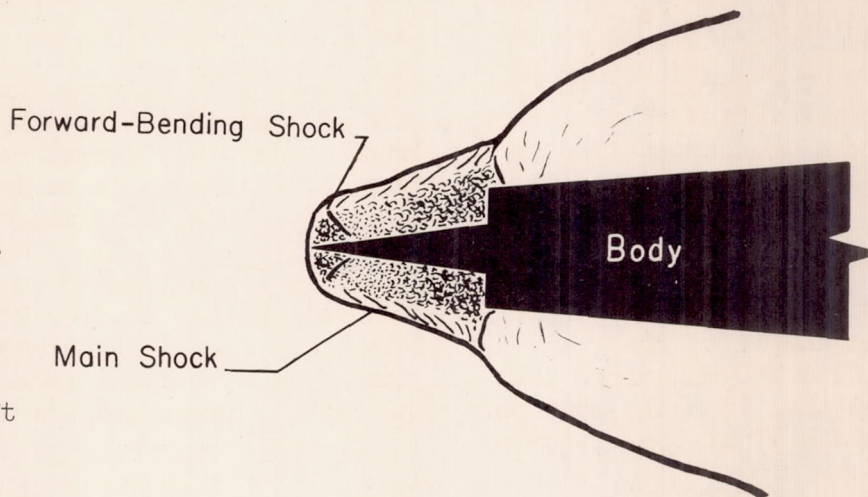
²This error was reduced below the $\pm 1^\circ$ error noted in connection with local recovery-temperature measurements by use of a more sensitive temperature-indicating instrument.

random intervals of time of the pulsating flow over the spike-nose body having the semicircular cutout ($\bar{X} = 2.0$ inches at $\alpha = 0^\circ$, $M_0 = 3.5$). The photographs so obtained have been arranged in the order in which the phenomenon apparently progresses and they are shown in figure 5. (The order chosen is in essential agreement with that deduced by Mair, ref. 8.) Thus figures 5(a) and 5(b) indicate a progressive piling up of turbulent air between the spike and the front of the model. In figure 5(c) the bow shock has swelled out substantially, and a high-speed reverse flow is indicated by the "forward bending" shock near the tip of the spike (see sketch). In figure 5(d) the bow shock has swelled further in the lateral direction but has begun to move aft on the spike.

Substantial turbulent air has collected between the bow shock and the forward bending shock near the tip. It is indicated in figure 5(e) that this turbulent mass has expanded, moved aft on the spike, and assumed a more or less doughnut-like

shape. In figures 5(f) and 5(g), this mass is seen to approach and discharge over the shoulder. In figure 5(h) it has passed a short distance down the model, and at the same time, turbulent flow is again beginning to pile up at the front of the model (as in fig. 5(a)). In between the turbulent masses, the body is immersed in a relatively thin but not altogether steady turbulent boundary layer (see figs. 5(e) and 5(g)).

Now it was conjectured that large-scale vortices would be discharged over a spike-nose body as a result of the pulsations in the flow at the nose, and that something resembling the proposed boundary-layer-vortex flow would occur on the body. These photographs lend credence to this conjecture. To illustrate, it is indicated in figure 5(d) that the reverse flow near the surface of the spike has coupled with an outward and rearward flow near the tip to start a large-scale vortical motion in the turbulent mass. This mass takes on a shape resembling a ring vortex (see fig. 5(e)) with probably zero velocity at its inner boundary (the surface of the spike) and some sizable downstream velocity at its outer boundary. The mass as a whole is moving downstream, and it discharges in a large-scale vortical motion over the shoulder of the model (fig. 5(g)). The turbulent mass continues down the model (fig. 5(h)) as something like a



large-scale ring-shaped vortex. Accordingly, this spike-nose configuration seems to provide at least a crude approximation to the proposed boundary-layer-vortex flow in the region aft of the nose.

Figures 5(a) and 5(h), when viewed together, suggest that the flow pattern tends to pulse between the quasi-steady, attached-shock-type obtained with an extended spike, and the steady, detached-shock-type characteristic of the plain blunt-nose body. This possibility was easily checked, and the results are shown in figure 6. Figures 6(a) and (c) are spark photographs of flow about the truncated cone model and the spike-nose model with semicircular cutout; the spike was extended sufficiently far to eliminate the large amplitude pulsations. Figures 6(b) and (d) are spark photographs of pulsating flow about the same spike-nose model (spike slightly retracted). The similarity between figures 6(a) and (b) and between figures 6(c) and (d) tends to verify qualitatively the limiting character of the pulsating flow pattern.

There are, no doubt, many other interesting characteristics of the pulsating flow associated with spike-nose configurations; some of these characteristics are discussed by Beastall and Turner (ref. 6). For the purposes of this paper, however, it was felt that a knowledge of one additional property would suffice. This property is the frequency with which vortices are discharged from the nose. An indication of this frequency was obtained at a Mach number of 3.5 using a hot-wire anemometer mounted just forward of the base of the heat-transfer model shown in figure 3. The anemometer revealed large amplitude pulses occurring at the rate of about 2600 per second. In the light of this observation and the photographs of figure 5, it is indicated that the pulsating flows created in these experiments were characterized by vortices on the order of 1 inch in diameter being discharged on the order of several thousand times per second. Now the important question is, do these vortices reduce the heat convected to a body in supersonic flow?

Heat-Transfer Characteristics

It was anticipated that aerodynamic cooling by large-scale vortices would reflect directly in the recovery temperature of a surface. That is to say, it was felt that the tendency of a large-scale vortex to abstract heat from a surface would lead to lower surface temperatures for the case of no net heat flow to (or from) the surface. Accordingly, the heat-transfer experiments were conducted as follows: First, the recovery temperatures of the test bodies were measured at a Mach number of 3.5 and zero angle of attack. In this regard, special attention was given to the effect of spike extension on the recovery temperatures of the spike-nose configurations. The optimum spike extension was taken as that which gave the lowest recovery temperatures. This spike extension, then, or one

slightly less, was used in all subsequent tests to determine recovery temperatures as a function of Mach number and angle of attack, and to determine heat transfer.

The measured recovery temperatures are reported in the form of recovery factors based on free-stream conditions, while the heat-transfer results are presented in the form of average heat-transfer coefficients. These two quantities are then treated together to facilitate a brief discussion of heat-transfer rates.

Recovery factors.- The effect of spike extension on the recovery factor at a typical point on the surface of the basic body is shown in figure 7. Results are presented for both the truncated cone with spike and the spike-nose configuration with semicircular cutout. These results are qualitatively similar in that the recovery factor is essentially constant at a relatively high value until the spike extends into the detached bow wave and starts the pulsating flow. With further spike extension the recovery factor falls off until a point is reached where the large amplitude pulsations can no longer be sustained.³ When this occurs the recovery factor rises more or less sharply to a value characteristic of normal boundary layers and remains essentially constant with further spike extension.

In the range of spike extensions where large amplitude pulsations occur, a hysteresis effect is encountered on the truncated cone with spike. Specifically, it is indicated that once pulsating flow ceases with increasing spike extension, a very substantial reduction in spike extension is required to re-establish the phenomenon. Note, too, that in the general region of the hysteresis effect, somewhat larger recovery factors are obtained during pulsation on the truncated cone with spike than with the semicircular cutout configuration. The semicircular cutout has the virtue, then, of eliminating the hysteresis effect and, simultaneously, of producing lower recovery factors under conditions of pulsation. In this regard it is thought that the sharp, forward-facing lip of the cutout may, in combination with the chamber effect, produce stronger and better developed vortices during pulsation, and tend to reduce the possibility of more than one type of flow for a given spike extension.⁴

³It is not to be implied that nonsteady motions, in general, will necessarily lower recovery temperatures. During the course of this investigation a variety of nonsteady boundary-layer flows were generated, but only a few (notably those characterized by large-scale vortices) reduced the recovery temperatures.

⁴The possibility of more than one type of flow for a given spike extension is not completely eliminated. This fact is indicated by the dashed line in figure 7 ($2.2 \leq \bar{X} \leq 2.6$) which denotes that both quasi-steady- and pulsating-type flows were observed to occur alternately.

So far the recovery factors have been considered at only one point on the surface of the spike-nose bodies. It is of interest now to study the recovery factors at various points along the body in the case of pulsating flow. For this purpose, a special nosepiece with integral spike and semicircular cutout was installed on the model. A schematic view of the body, with thermocouple locations, and the test results at a Mach number of 3.5 are shown on figure 8. The spike extension is about three-fourths of that required for obtaining minimum recovery factors. It is observed first that the recovery factors rise from a relatively low value near the center of the spike to a high value in the neighborhood of the semicircular cutout. The low recovery factors may be associated with the discharge of large-scale vortices from the spike (see fig. 5). This possibility is brought to mind by the work of Eckert and Weise (ref. 9) and Ryan (ref. 10) which revealed that low temperatures are obtained on that portion of transverse cylinders discharging vortices in subsonic flow.

On the afterbody something like the proposed boundary-layer-vortex flow has been developed, and it is observed that the recovery factors are uniformly low, varying from about 0.72 to about 0.75.

It is of interest to compare the recovery factors on the afterbodies of the test models. This is done in figure 9 where recovery factor is shown as a function of distance from the shoulder of the basic body. The spike extensions are those for minimum recovery factor; the models with movable spikes were employed to obtain these data. It is seen that the recovery factor first decreases and then increases slowly with distance along the spike-nose bodies, while it remains more or less constant at values characteristic of normal-boundary-layer flows on the truncated cone. The maximum reduction in recovery factor due to spike extension is from about 0.91 to about 0.68 and it occurs near the 1-inch location on the spike-nose configuration with semicircular cutout. The corresponding reduction in recovery temperature would be from 1150° F to 870° F for a vehicle in flight at a Mach number of 3.5 in air at 40° F ambient temperature. Large-scale vortices offer promise, then, of substantially reducing the recovery temperatures of aircraft in flight at high supersonic speeds.

In order to provide more information on this possibility, the recovery factors over the afterbodies of the models were determined at small angles of attack for a Mach number of 3.5. These results are presented in figure 10 for two values of the meridian angle θ . Data for the truncated cone are shown in figure 10(a) and it is seen that there is little effect of angle of attack. Figures 10(b) and 10(c) show the recovery factors for the two spike-nose configurations. It should be noted that the spike extension for these tests was less than that for minimum recovery temperatures at zero angle of attack. This situation reflects the fact that pulsating flow could not be maintained at angle of attack when the optimum spike extension for zero incidence was used - that is

to say, the spike had to be retracted slightly at angle of attack in order to sustain the pulsations. Accordingly, the recovery temperatures are not as low as those obtainable at $\alpha = 0^\circ$. Generally, the effect of angle of attack is to increase surface temperatures on the windward side and to decrease them on the leeward side of a body. At small α 's the temperatures on the sides of the bodies are, as would be expected, more or less unchanged. The body with semicircular cutout has the advantage that temperatures are more uniform and generally lower.^{5,6}

Up to this point, attention has been restricted to surface-temperature phenomena at a Mach number of 3.5. The effect of Mach number on recovery factor for the test models is shown in figure 11. These results were determined at zero angle of attack for Mach numbers from 3 to 5.

The recovery factors for the afterbody of the truncated cone (fig. 11(a)) remain high. The recovery factors on the afterbodies of the spike-nose models are shown in figures 11(b) and 11(c). These data were obtained with the movable spike models, and the spike extensions were such as to give minimum recovery temperature at each test Mach number. The spike nose with semicircular cutout causes the largest reductions in recovery factor, which suggests that this configuration is the most effective vortex generator over the test Mach number range. The fact that the lowest recovery factors for both bodies were obtained at $M_0 = 3.5$ is not viewed as an indication that there is anything especially unique about this Mach number. Rather, it is thought that this is a result of the model designs.

Heat-transfer coefficients.- Only a limited number of heat-transfer measurements were made. Specifically, they were comprised of the total heat transfer from the models (including the nosepiece) and the heat transfer from their afterbodies at a Mach number of 3.5 and zero incidence. The experimental results are presented in figure 12 where the average heat-transfer coefficients are shown as a function of the difference between indicated recovery temperature and indicated wall temperature. These temperatures are referred to as "indicated" temperatures because they were measured in the interior near the base of a model rather than at points on the surface⁷ (figs. 3 and 4).

⁵It will be noted in figure 10(c) that the recovery factors at $\theta = 0^\circ$ and $\theta = 90^\circ$ do not agree at the first thermocouple on the model with the semicircular cutout. It is believed that this discrepancy is due to variations in the degree of contact between the nosepiece and the thin-walled section (see footnote 1 and fig. 2).

⁶It is possible that some advantage might accrue if the spike nose were kept aligned with the stream, independent of the incidence of the main body. In this manner the general level of surface temperatures might be kept closer to the low zero-lift values by obtaining pulsating flow with greater spike extension.

The average heat-transfer coefficients based on measured total heat transfer from the models are shown in figure 12(a). The spike on the basic body raises the average heat-transfer coefficients while the spike plus semicircular cutout lowers them. In any case the changes are fairly small, varying from about 5 to -10 percent.⁸ The average heat-transfer coefficients for the afterbodies of the models are shown in figure 12(b). It is seen that the effect of the spike is to raise these coefficients as much as 20 percent.

Heat-transfer coefficients are especially useful if they are constant, independent of wall temperature. It is to be expected that they would be constant for normal boundary-layer flows (and not too large a temperature change) and, on the basis of the data presented in figure 12, it would appear that they are also more or less constant for the pulsating flows. This will be assumed to be the case and the combined significance of the measured heat-transfer coefficients and recovery factors will be interpreted in terms of heat-transfer rates.

Heat-transfer rates.- This discussion is facilitated by use of the elementary heat flow equation

$$q = h(T_R - T_W) \quad (1)$$

In this expression q is the rate of heat transfer per unit area, h is the heat-transfer coefficient, and T_R and T_W are the recovery and wall temperatures, respectively. The recovery temperature may be written

$$T_R = T_0 \left(1 + \frac{\gamma - 1}{2} M_0^2 R \right) \quad (2)$$

where T_0 is the free-stream static temperature, γ is the ratio of specific heats, M_0 is the free-stream Mach number and R is the recovery factor. Combining equations (1) and (2) yields the relation

$$q = h \left[\frac{\gamma - 1}{2} M_0^2 R T_0 + (T_0 - T_W) \right] \quad (3)$$

⁷Use of these temperatures is thought permissible for the comparative purposes of this report.

⁸Corresponding heat-transfer coefficients for the models with spikes extended to give quasi-steady flow were not appreciably different from those given in figure 12(a).

It is anticipated that surface temperatures in flight are not likely to take on values less than the ambient temperature. In this event it follows from equation (3) that heat-transfer rates are not likely to exceed those given by the expression

$$q_{\max} = \frac{\gamma - 1}{2} M_0^2 T_0 hR \quad (4)$$

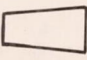
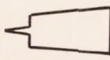
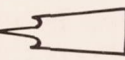
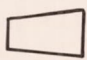
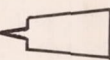
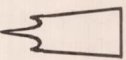
or, as it suffices for this discussion,

$$q_{\max} \sim hR \quad (5)$$

That is to say, the maximum rate of heat transfer per unit area is simply proportional to the product of the heat-transfer coefficient and the recovery factor. It is this result which will be used in the following discussion.

First a comparison will be made of the average values of q_{\max} for the complete models. All necessary information (in the sense of eq. (5))

Table I

| | Complete model | | | Model afterbody | | |
|-----------------|--|--|--|--|--|--|
| Body shape |  |  |  |  |  |  |
| h | 0.0072 | 0.0077 | 0.0067 | 0.0085 | 0.0103 | 0.0097 |
| R _i | .910 | .778 | .767 | .913 | .758 | .745 |
| hR _i | .0066 | .0060 | .0051 | .0078 | .0078 | .0072 |

is given in figure 12 and it has been collected in table I. The results for the truncated cone will be used as a basis of comparison to determine the effects of pulsating flow on heat-transfer rate. From the data in the table it can be deduced that the spike on the truncated cone reduces the average q_{\max} by about 9 percent and the spike plus semicircular cutout reduces the average q_{\max} by about 22 percent. In this respect, then, the addition of the semicircular cutout is definitely beneficial.

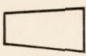
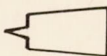
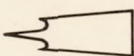
Consider now the afterbody heat-transfer rates. With the afterbody of the truncated cone as a basis of comparison, it is deduced that the addition of the spike does not change the average q_{\max} , while the addition of the spike plus semicircular cutout reduces the average q_{\max} by about 7 percent. On the basis of these few results then, the pulsating flow appears less effective in reducing the average rate of heat transfer per unit area for the afterbody than it is in reducing the corresponding quantity for the complete models. It is to be recognized, of course, (see eq. (1)) that the percentage reduction in heat-transfer rates will be greater with increasing wall temperature.

It is of interest now to consider the rate of total heat transfer to the models. It follows from equation (5) that the proportionality relation for the maximum values of this quantity is

$$Q_{\max} \sim hRS \quad (6)$$

That is, the maximum total heat-transfer rate is proportional to the product of the heat-transfer coefficient, the recovery factor, and surface area. This product is shown in table II for the complete models where the values of heat-transfer coefficient times recovery factor were taken from table I.

Table II

| Body shape |  |  |  |
|------------|---|---|--|
| S | 0.153 | 0.157 | 0.177 |
| hR_1S | .00100 | .00094 | .00091 |

Evidently Q_{\max} is lowest for the truncated cone with semicircular cut-out and spike, being about 9 percent less than that of the truncated cone.

In the case of the heat-transfer rates for the afterbodies of the models, the values of Q_{\max} would bear the same relation for the models as the values of q_{\max} already discussed since each model had the same afterbody surface area. It should be noted, too, that these and the previous considerations of heat transfer apply qualitatively at small angles of attack since, by symmetry, the average rate of heat transfer should vary only slightly about zero angle of attack.

Aerodynamic Characteristics

The lift, drag, and pitching-moment characteristics of the test bodies were determined for angles of attack up to 4° at a Mach number of 3.5. These results are presented in figure 13. The zero-lift drag characteristics were obtained over the test Mach number range from 3 to 5 and the results are presented in figure 14.

First consider the effects of angle of attack on lift and foredrag at a Mach number of 3.5. It is evident from figure 13(a) that the effect of a spike is to increase lift by a factor of about 2 over that for the truncated cone. The spike plus semicircular cutout decreases the foredrag of the truncated cone by about one-third (fig. 13(b)).

Now as regards pitching moment, it is noted in figure 13(c) that the moment about the base is slightly less in the case of the truncated cone than in the case of the spike-nose models. The center of pressure, figure 13(d), varies only slightly with angle of attack and is not appreciably ahead of the 50-percent-length station for any model.

The zero lift-drag characteristics of the test bodies were measured over the Mach number range. The measured foredrag coefficients are shown in figure 14(a), and the measured total drag coefficients are shown in figure 14(b).⁹

It is observed that, in general, the foredrags increase slightly with Mach number, while the total drags are more or less unaffected by Mach number. The configuration with 2-inch spike extension and semicircular cutout has the lowest drag of the blunt-nose bodies.

CONCLUDING REMARKS

It was conjectured that convective heat transfer to a surface in supersonic flow might be reduced by periodically imposing a large-scale vortical motion on the boundary layer. Results of experiments were presented which tended to confirm this conjecture. In particular, marked reductions in heat transfer and recovery factor were obtained on two bodies of revolution immersed in a flow resembling the boundary-layer-vortex model. While this work is of a very preliminary nature, it has several implications which are worthy of note. For one thing, aerodynamic cooling by large-scale vortices might prove especially effective in the case of ballistic-type vehicles where aerodynamic heating characteristics are of primary importance (see ref. 5).

The application of vortex cooling to other types of supersonic aircraft is less clear. Nevertheless, the experiments of this paper do indicate that large-scale vortices may constitute a practical means of substantially reducing aerodynamic heating in flight at high supersonic speeds. Further investigations of this possibility appear warranted.

Ames Aeronautical Laboratory
National Advisory Committee for Aeronautics
Moffett Field, Calif., Dec. 13, 1954

⁹The drag data for the model with semicircular cutout correspond to two different spike extensions. The spike extension of 1.6 inches was used to obtain the major part of heat-transfer and aerodynamic data for this configuration. The spike extension of 2 inches gave near minimum recovery factors (see fig. 7).

APPENDIX

NOTATION

- A cross-sectional area of base of body, sq ft
- C_D drag coefficient, $\frac{D}{\frac{\rho_0 V_0^2}{2} A}$
- C_L lift coefficient, $\frac{L}{\frac{\rho_0 V_0^2}{2} A}$
- C_m pitching-moment coefficient (moment about body base), $\frac{\text{moment}}{\frac{\rho_0 V_0^2}{2} A l}$
- c.p. center of pressure, percent of basic body length from base
- D drag, lb
- h heat-transfer coefficient, $\frac{q}{T_r - T_w}$, Btu/sq ft, sec, °R
- L Lift, lb
- l length of body (exclusive of spike-nose assembly), ft
- M_0 free-stream Mach number
- Q rate of heat transfer, Btu/sec
- q average rate of heat transfer per unit area, $\frac{Q}{S}$, Btu/sq ft, sec
- R recovery factor, $\frac{T_r - T_0}{T_s - T_0}$
- S surface area, sq ft
- T_0 free-stream static temperature, °R
- T_r recovery temperature, °R
- T_s stagnation temperature, °R
- T_w wall temperature, °R

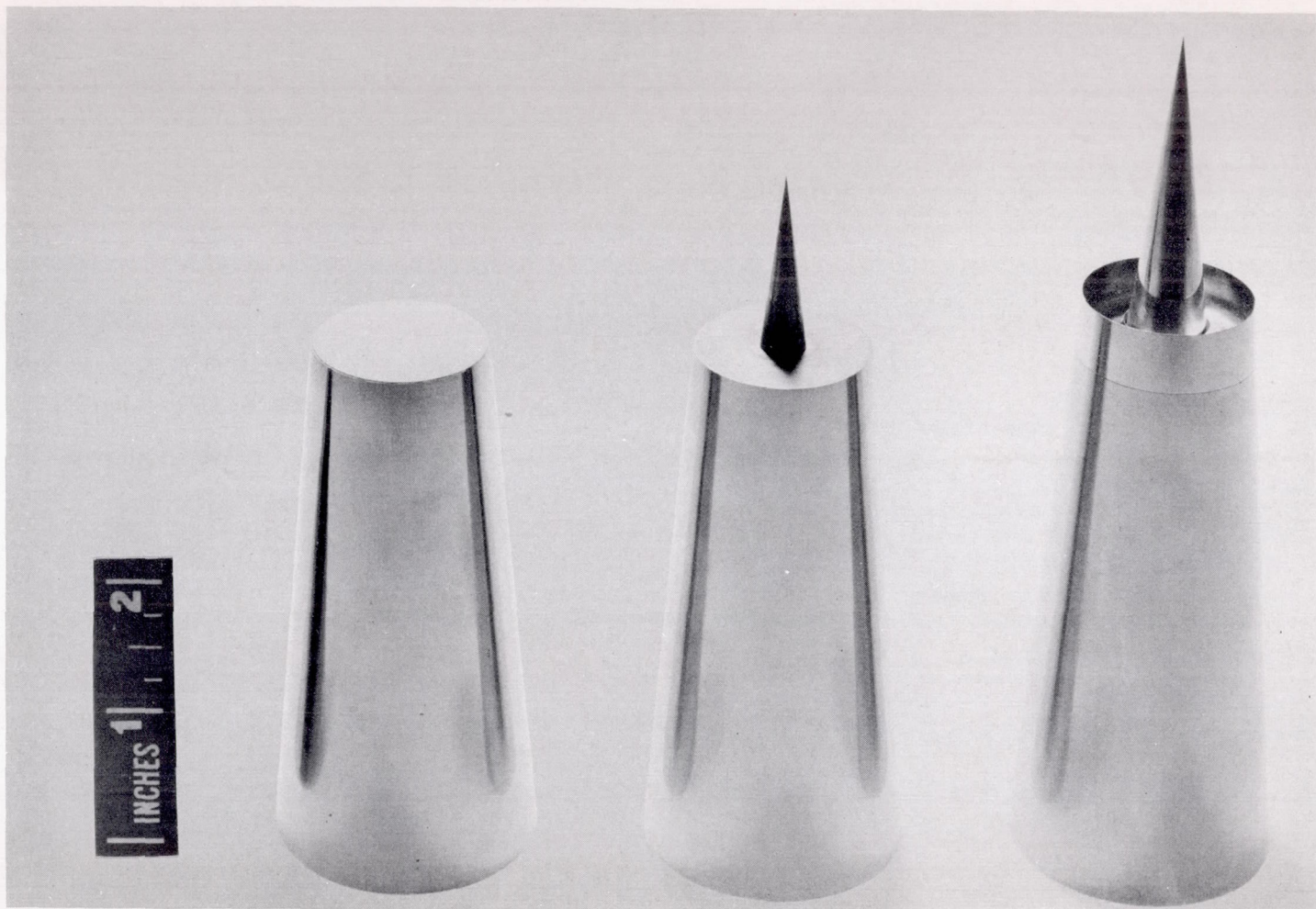
| | |
|-----------|--|
| V_0 | free-stream velocity, ft/sec |
| X | distance from shoulder of basic body to thermocouple, in. (See fig. 2) |
| \bar{X} | distance from front of body to tip of spike, in. (See fig. 2) |
| α | angle of attack, deg |
| ρ_0 | free-stream density, slugs/cu ft |
| θ | meridian angle around body (measured from windward side of body), deg |
| γ | ratio of specific heat at constant pressure to specific heat at constant volume |

Subscripts

| | |
|---|--------------------------------------|
| a | body aft of nose (exclusive of base) |
| f | complete body (exclusive of base) |
| i | indicated temperature |
| t | total drag (including base drag) |

REFERENCES

1. O'Sullivan, William J., Chauvin, Leo T., and Rumsey, Charles B.: Exploratory Investigation of Transpiration Cooling to Alleviate Aerodynamic Heating on an 8° Cone in a Free Jet at a Mach Number of 2.05. NACA RM L53H06, 1953.
2. Smith, John W.: Effect of Diffusion Fields on the Laminar Boundary Layer. Jour. Aero. Sci., vol. 21, no. 3, pp. 154-162, Mar. 1954.
3. Dorrance, William H., and Dore, Frank J.: The Effect of Mass Transfer on the Compressible Turbulent Boundary-Layer Skin Friction and Heat Transfer. Jour. of Aero. Sci., vol. 21, no. 6, pp. 404-410, June 1954.
4. Rubesin, Morris W.: An Analytical Estimation of the Effect of Transpiration Cooling on the Heat-Transfer and Skin-Friction Characteristics of a Compressible, Turbulent Boundary Layer. NACA TN 3341, 1954.
5. Allen, H. Julian, and Eggers, A. J., Jr.: A Study of the Motion and Aerodynamic Heating of Missiles Entering the Earth's Atmosphere at High Supersonic Speeds. NACA RM A53D28, 1953.
6. Beastall, D., and Turner, J.: The Effect of a Spike Protruding In Front of a Bluff Body at Supersonic Speeds. R.A.E. TN No. Aero. 2137, Jan. 1952.
7. Eggers, A. J., Jr., and Nothwang, George J.: The Ames 10- by 14-Inch Supersonic Wind Tunnel. NACA TN 3095, 1954.
8. Mair, W. A.: Experiments on Separation of Boundary Layers on Probes in Front of Blunt-Nosed Bodies in a Supersonic Air Stream. Phil. Mag., vol. 43, Seventh Series, no. 342, pp. 695-716, July 1952.
9. Eckert, E., and Weise, W.: Measurement of Temperature Distribution on the Surface of Unheated Bodies in High Velocity Flow. Forschung auf dem Gebiete des Ingenieurwesens, vol. 13, pp. 246-254, 1942.
10. Ryan, Lloyd F.: Experiments on Aerodynamic Cooling. Mitteilungen Aus Dem Institut Fur Aerodynamik an Der Eidgenossischen Technischen Hochschule in Zurich, Nr. 18.



CONFIDENTIAL

Truncated Cone
(Basic Body)

Truncated Cone
With Spike

Truncated Cone
With Spike and
Semicircular Cutout

A-19670.1

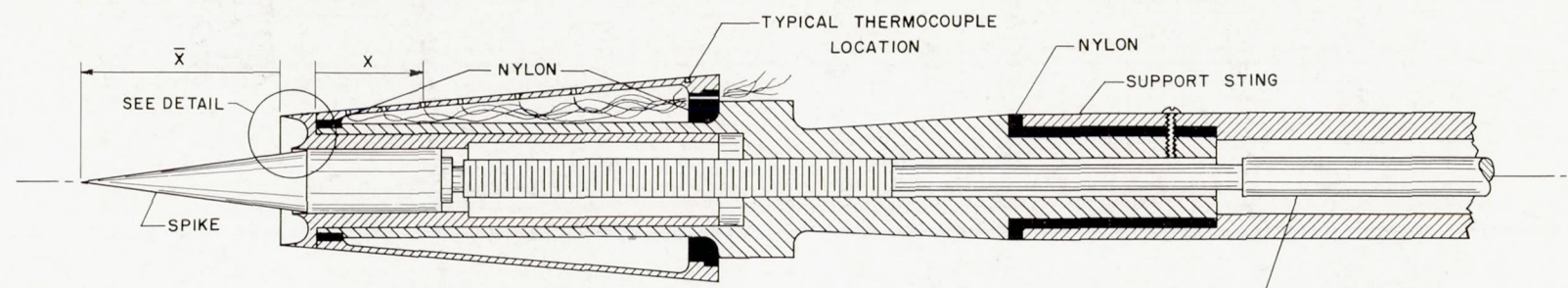
Figure 1.- Model shapes.



TRUNCATED CONE WITH SPIKE

DETAIL OF SEMICIRCULAR CUTOUT NO SCALE

CONFIDENTIAL



TRUNCATED CONE WITH SPIKE AND SEMICIRCULAR CUTOUT

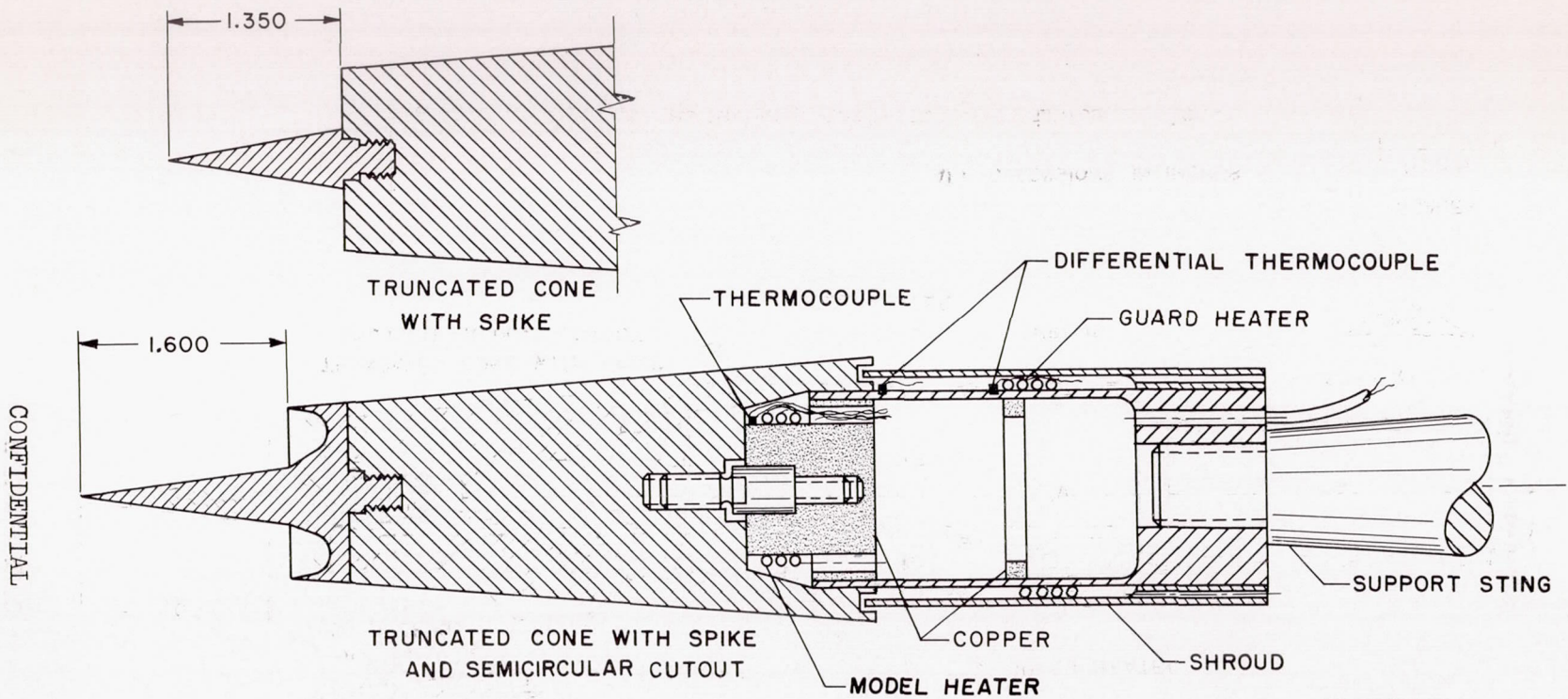
ALL DIMENSIONS IN INCHES.



SCALE: 1 INCH

Figure 2.- Typical recovery-temperature installation.

CONFIDENTIAL



CONFIDENTIAL

ALL DIMENSIONS IN INCHES.

SCALE:

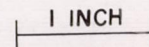
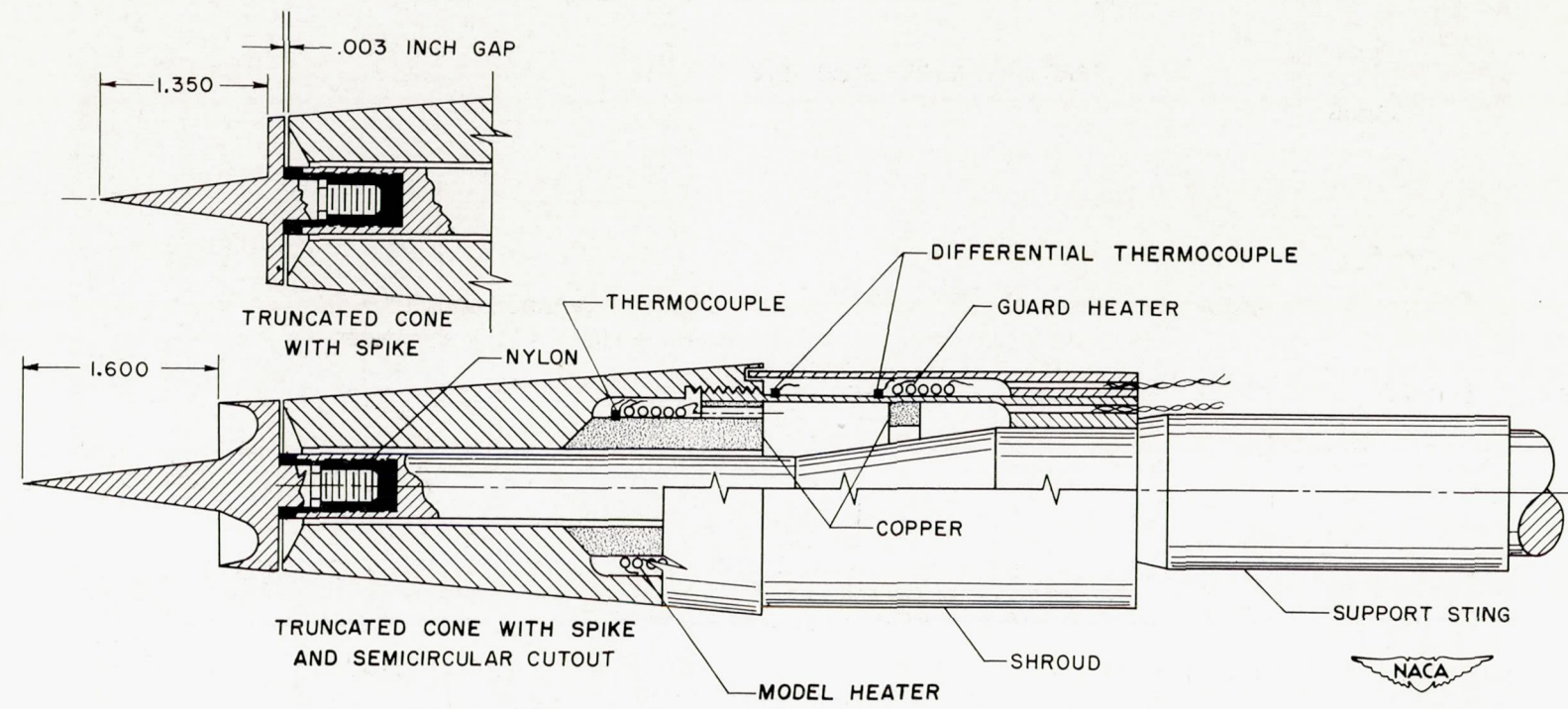


Figure 3.- Typical total heat-transfer installation.

CONFIDENTIAL



CONFIDENTIAL

ALL DIMENSIONS IN INCHES.

SCALE :

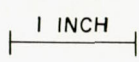
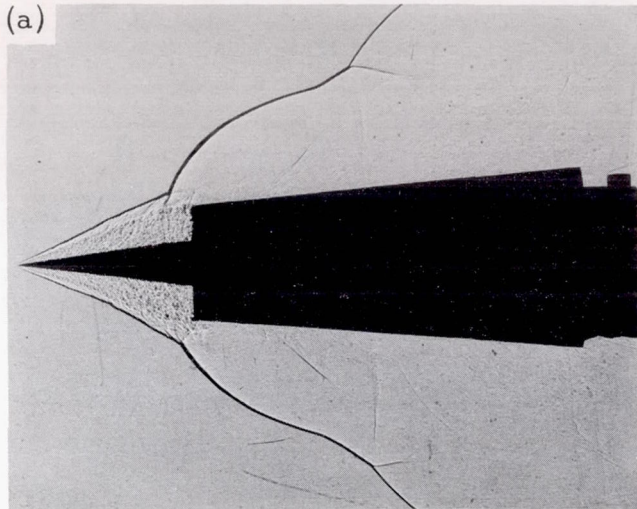
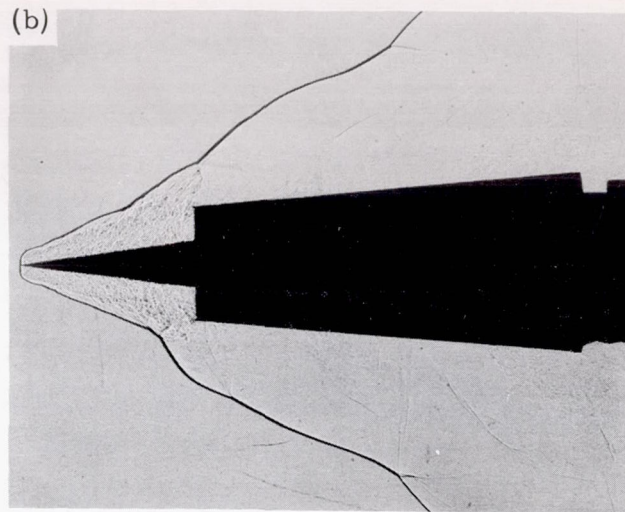


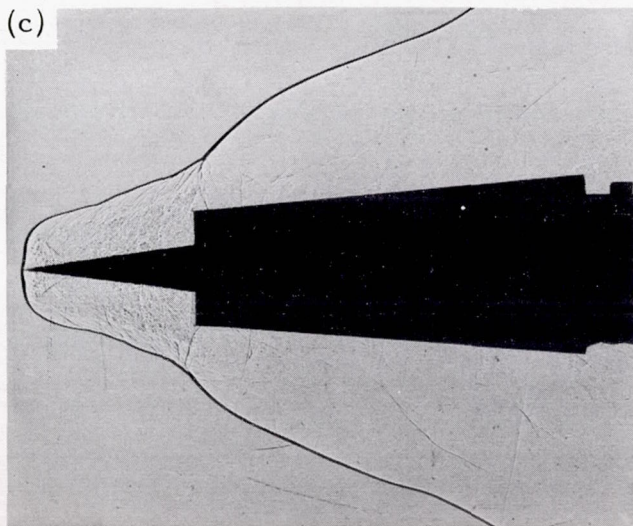
Figure 4.- Typical afterbody heat-transfer installation.



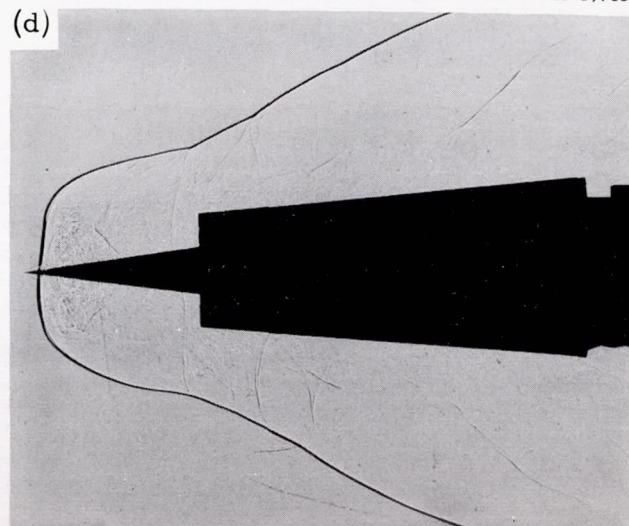
A-19744



A-19745

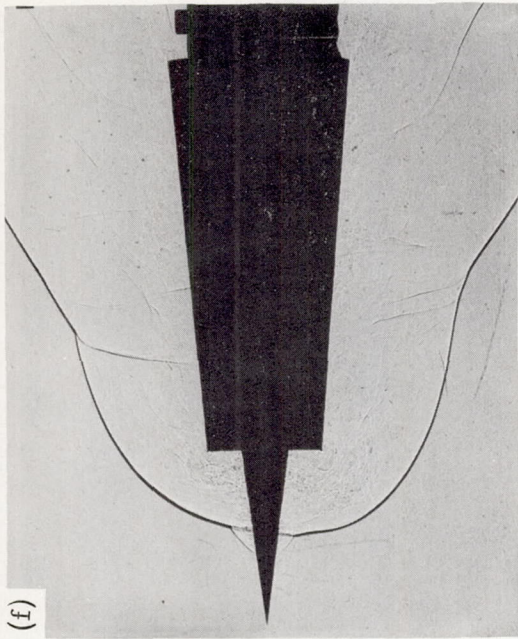


A-19746



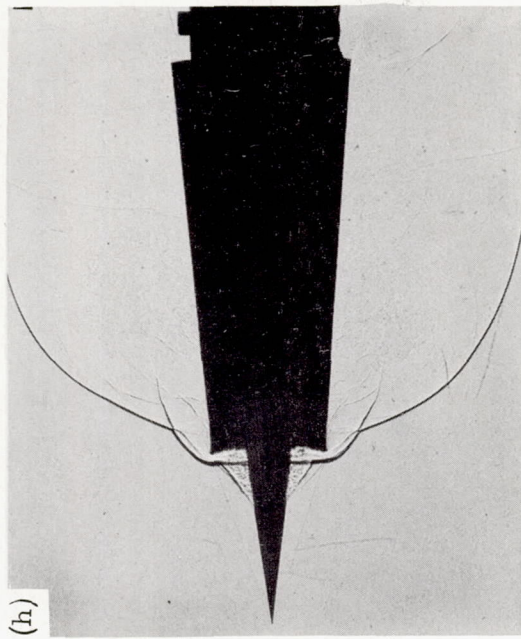
A-19747

Figure 5.- Photographs of nonsteady flow phenomena about the spike-nose configuration with semicircular cutout ($\bar{X} = 2.000$ inches).



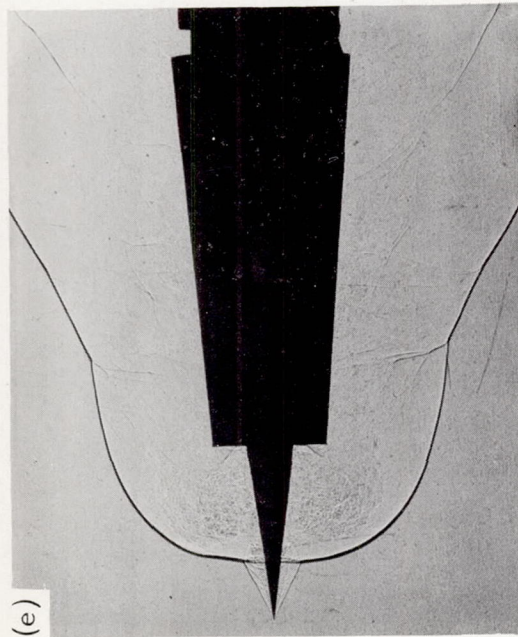
A-19749

(f)



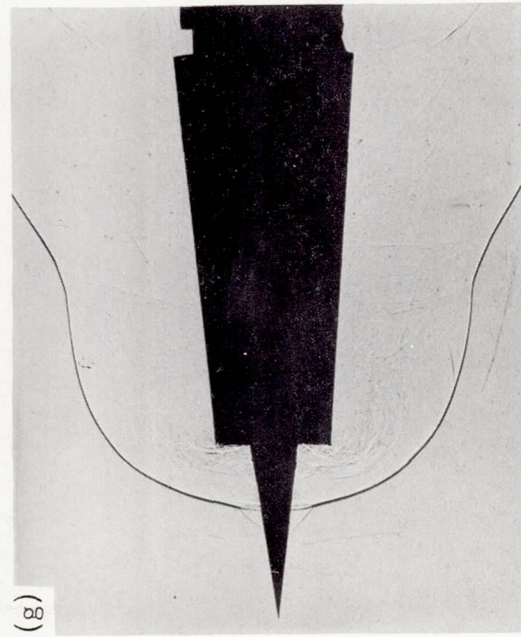
A-19752

(h)



A-19748

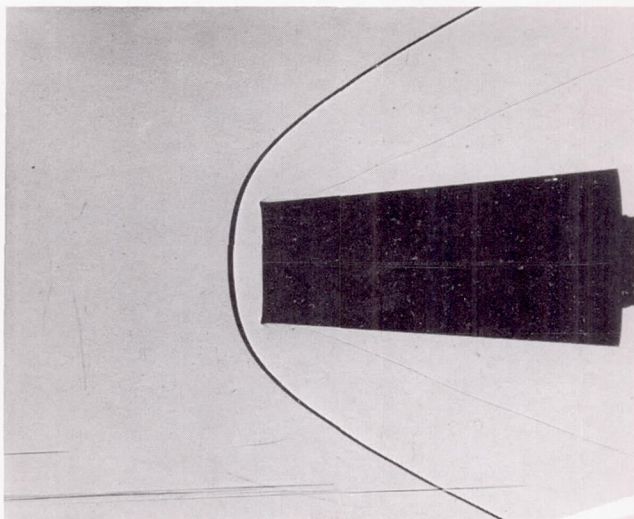
(e)



A-19750

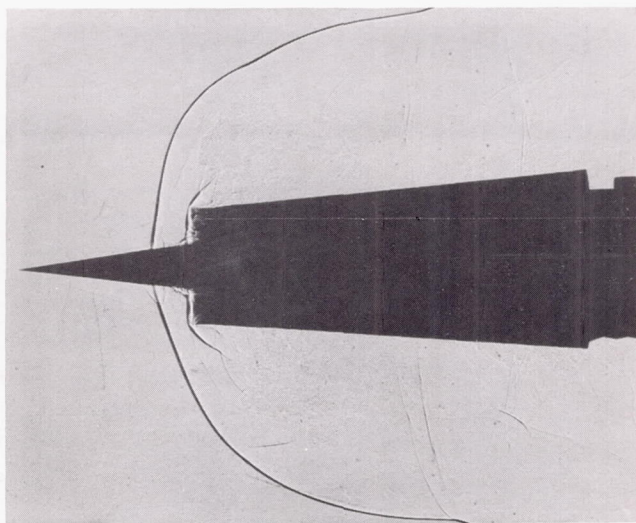
(g)

Figure 5.- Concluded.



A-19754

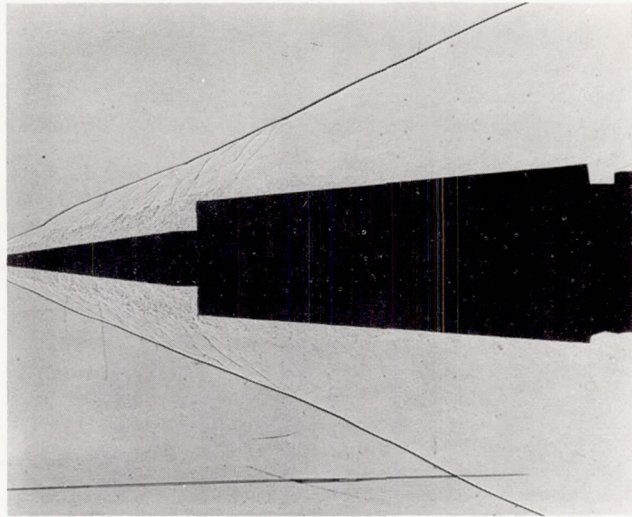
(a) Flow about truncated cone.



A-19751

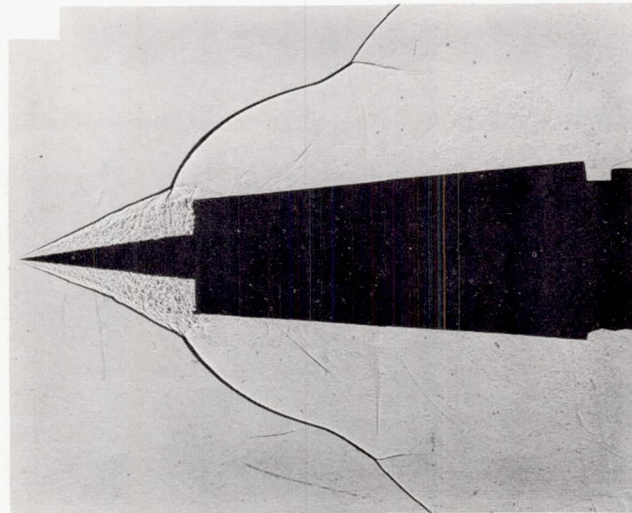
(b) Nonsteady flow about spike-nose body with semicircular cutout-detached shock ($\bar{X} = 2.000$ inches).

Figure 6.- Photographs showing comparison between steady and nonsteady flows.



A-19753

(c) Quasi-steady flow about spike-nose body with semicircular cutout ($\bar{X} = 2.700$ inches).



A-19744

(d) Nonsteady flow about spike-nose body with semicircular cutout-attached shock ($\bar{X} = 2.000$ inches).

Figure 6.- Concluded.

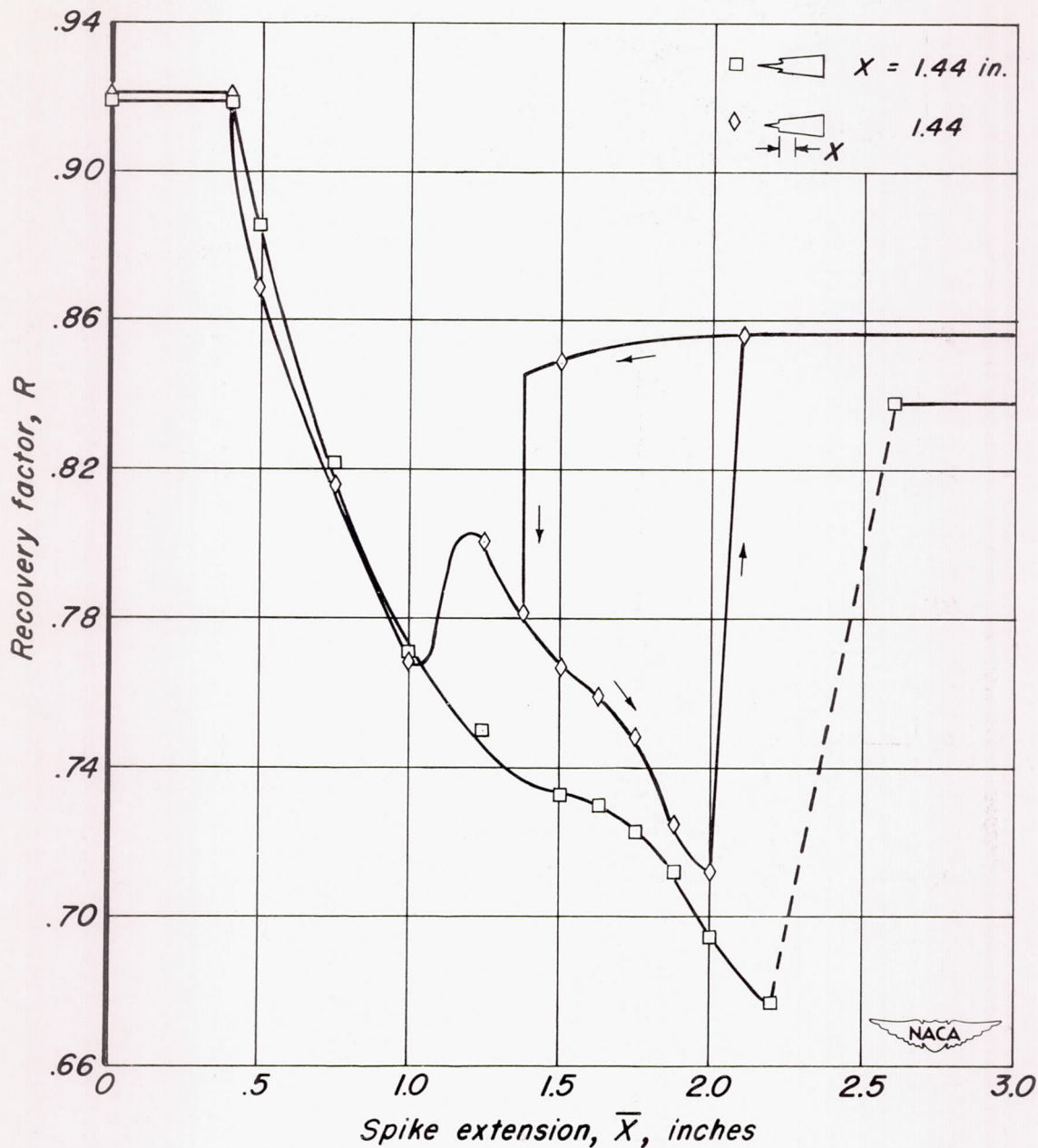


Figure 7.- Effect of spike extension on recovery factor of the spike-nose configurations; $\alpha = 0^\circ$, $M_0 = 3.5$.

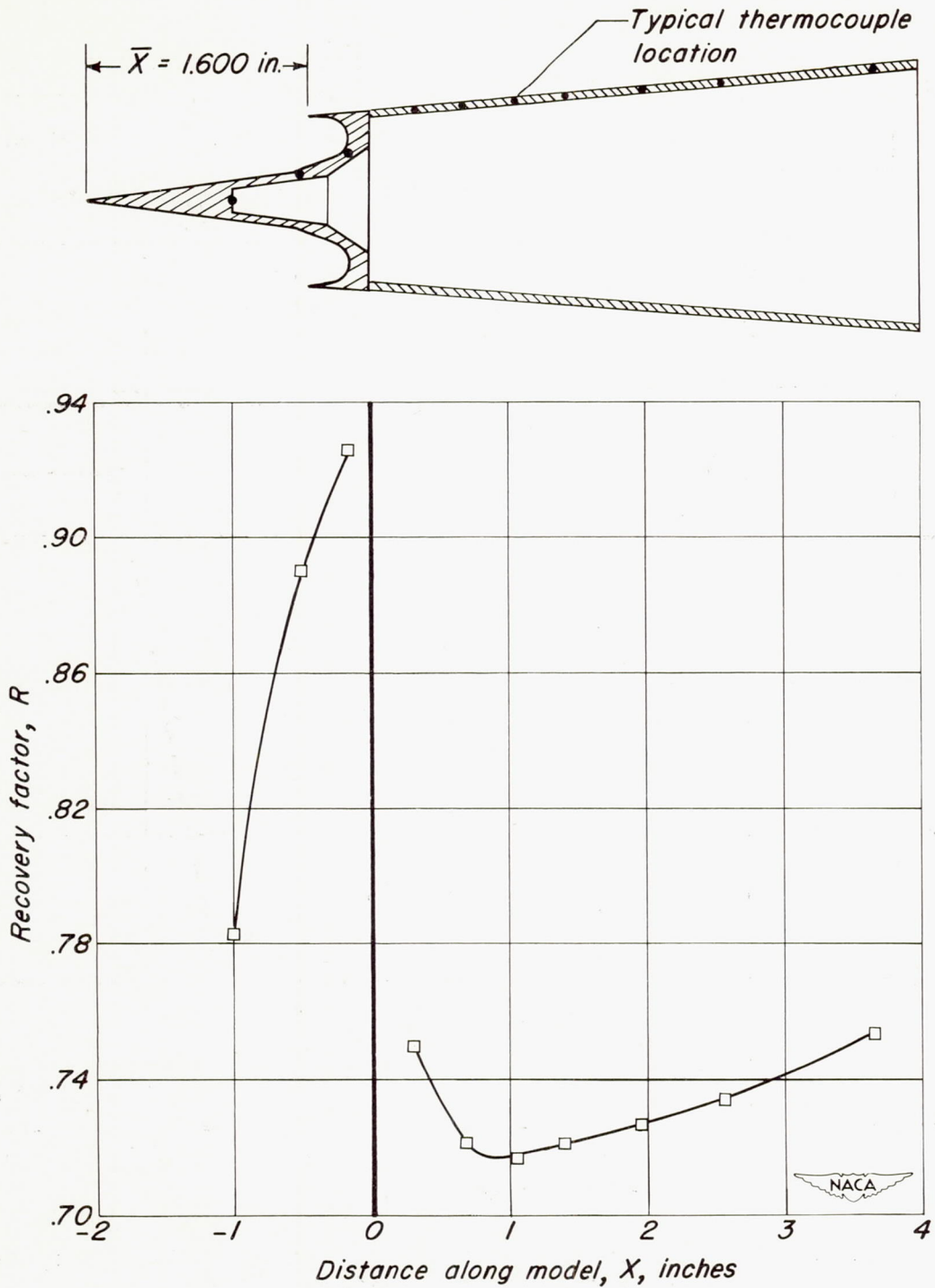


Figure 8.- Variation of recovery factor along the surface of the spike-nose configuration with semicircular cutout; $\alpha = 0^\circ$, $M_0 = 3.5$.

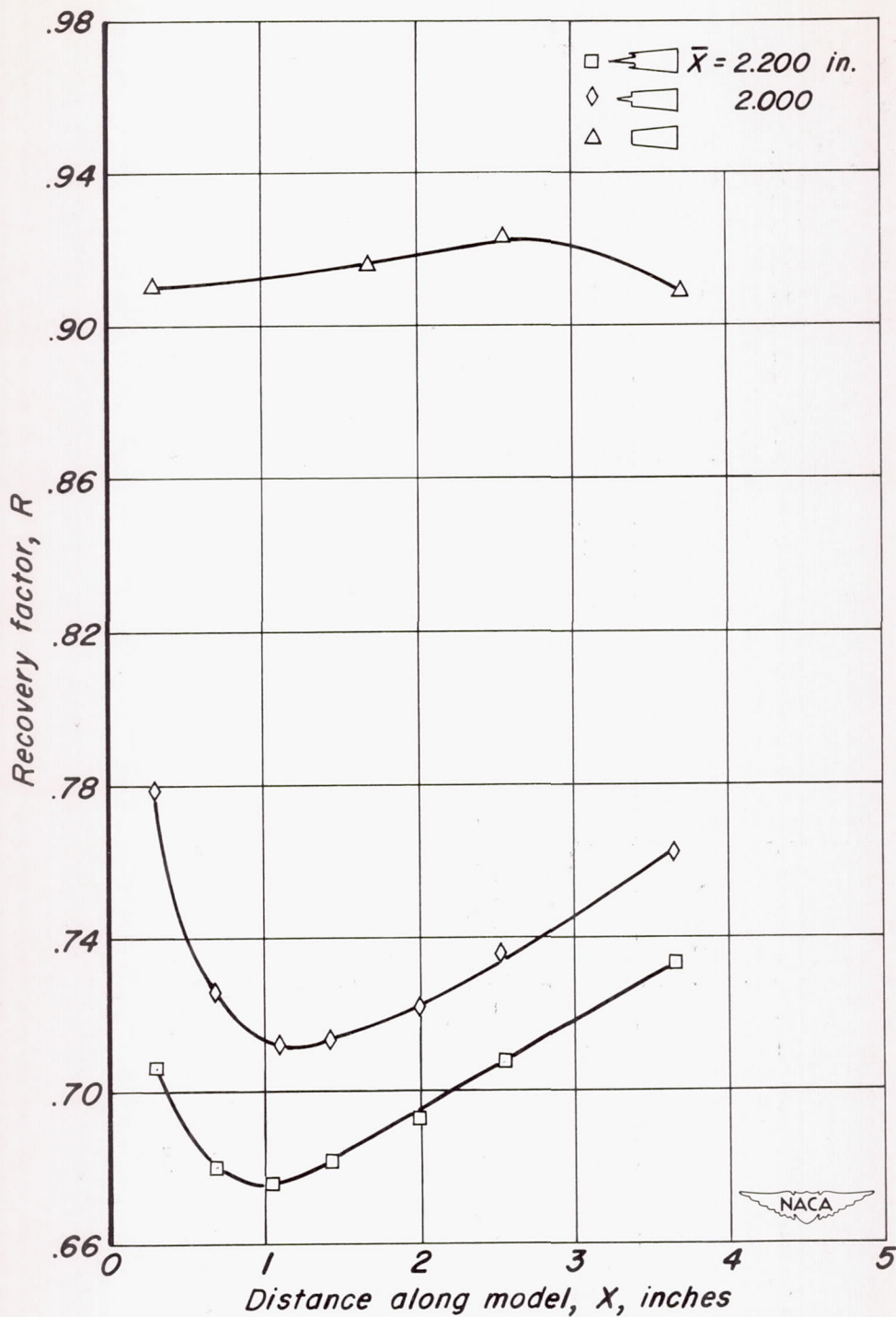


Figure 9.- Comparison of recovery factors for different body shapes; $\alpha = 0^\circ$, $M_0 = 3.5$.

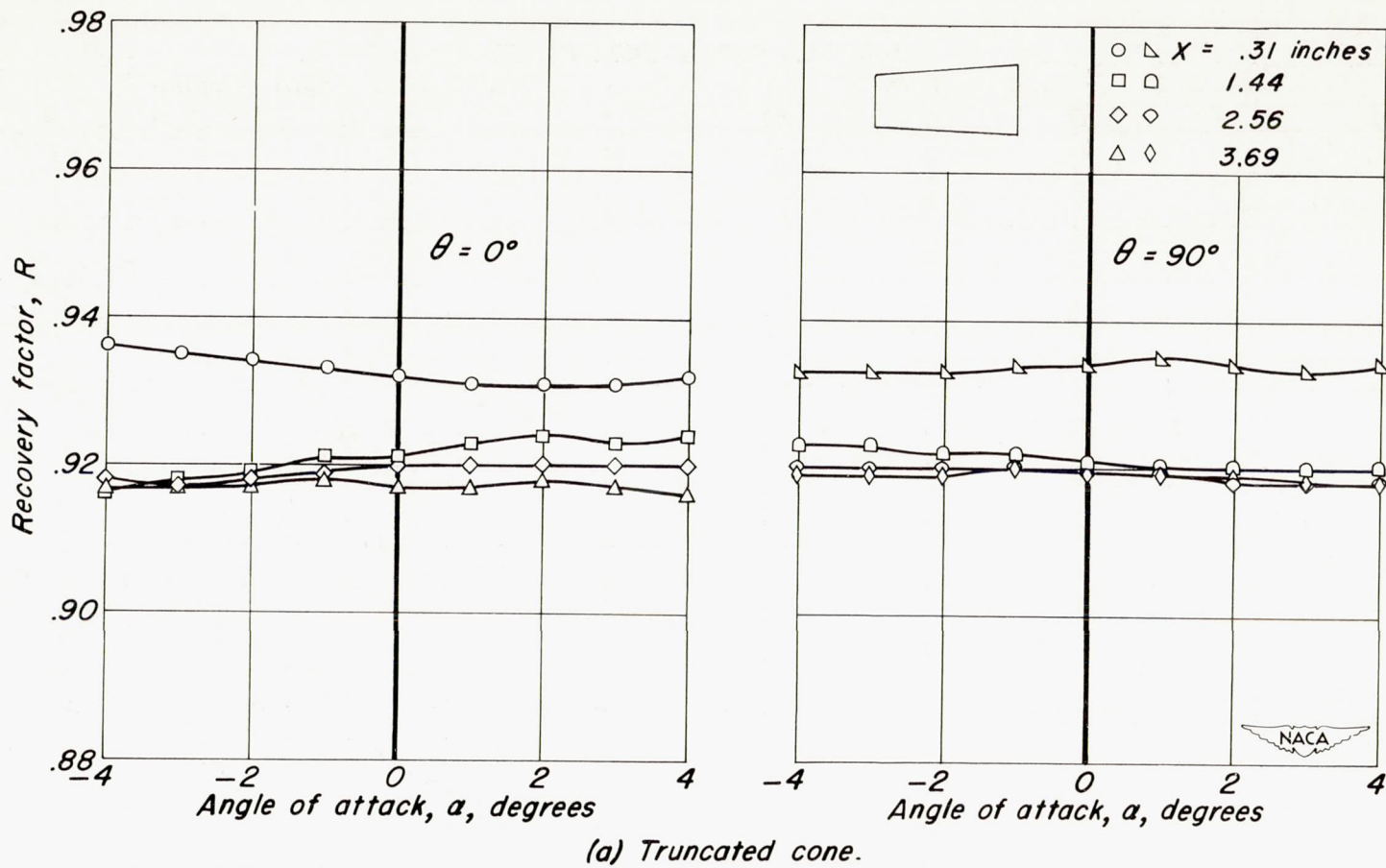
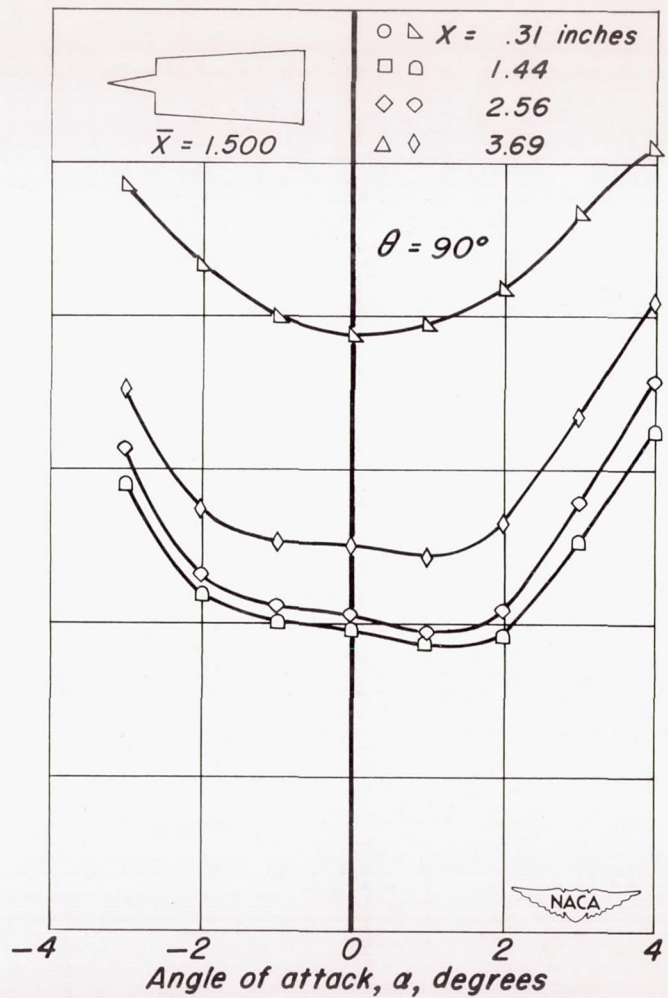
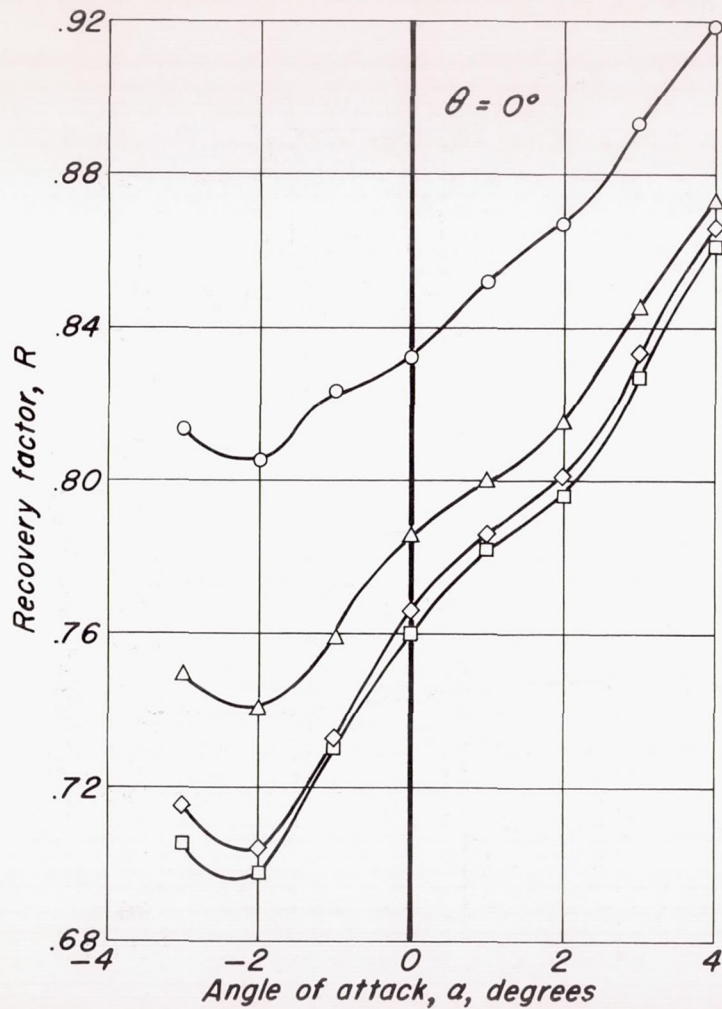
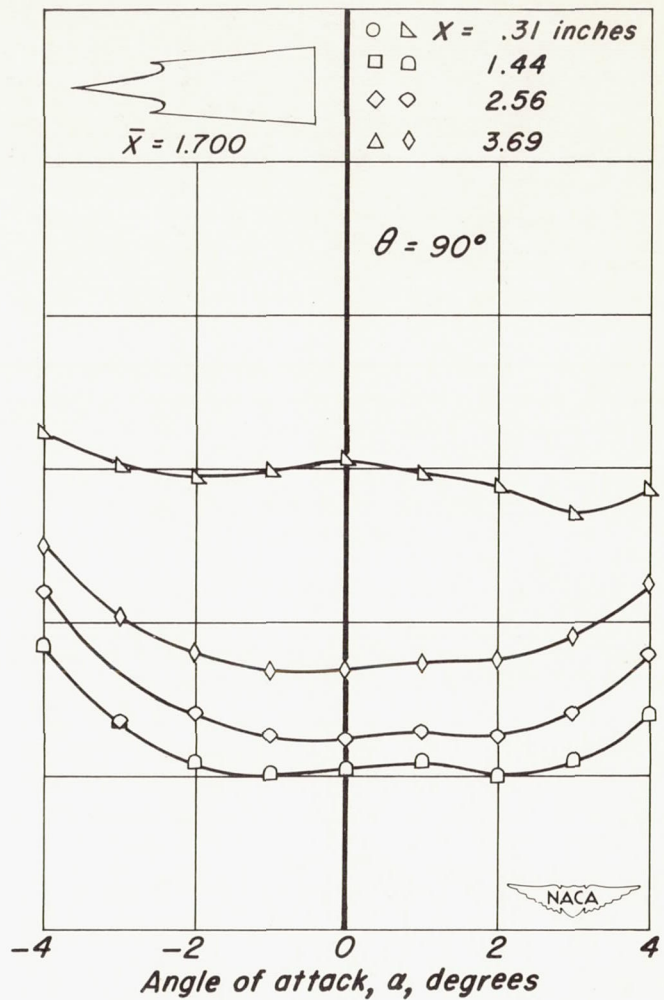
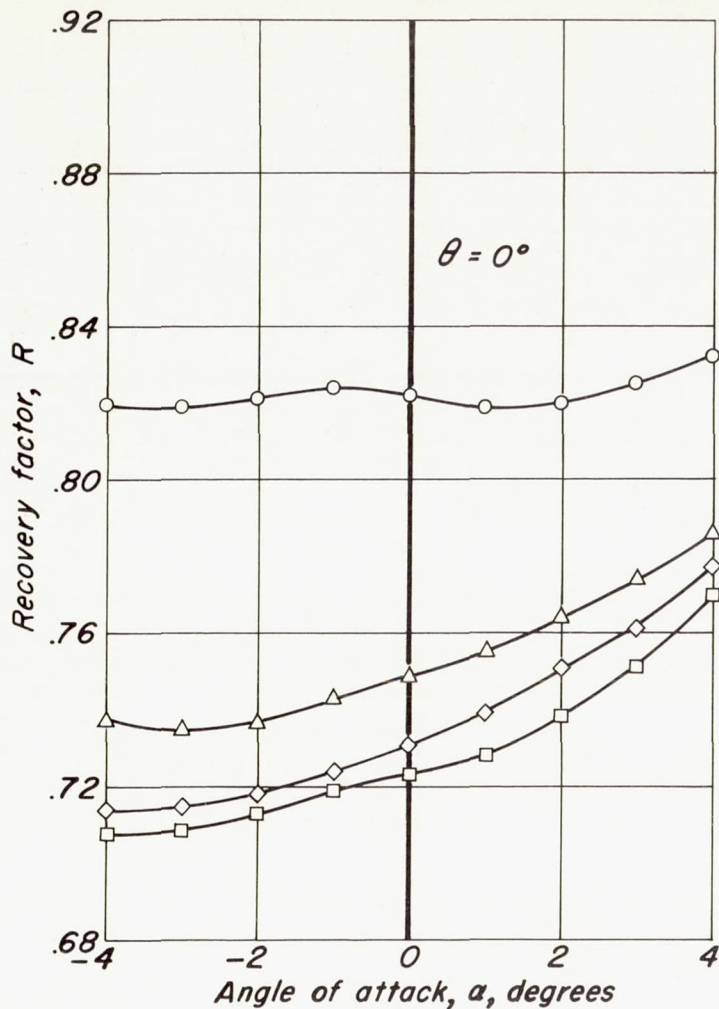


Figure 10.- Effect of angle of attack on recovery factor; $M_0 = 3.5$.



(b) Truncated cone with spike

Figure 10.- Continued.



(c) Truncated cone with spike and semicircular cutout.

Figure 10.- Concluded.

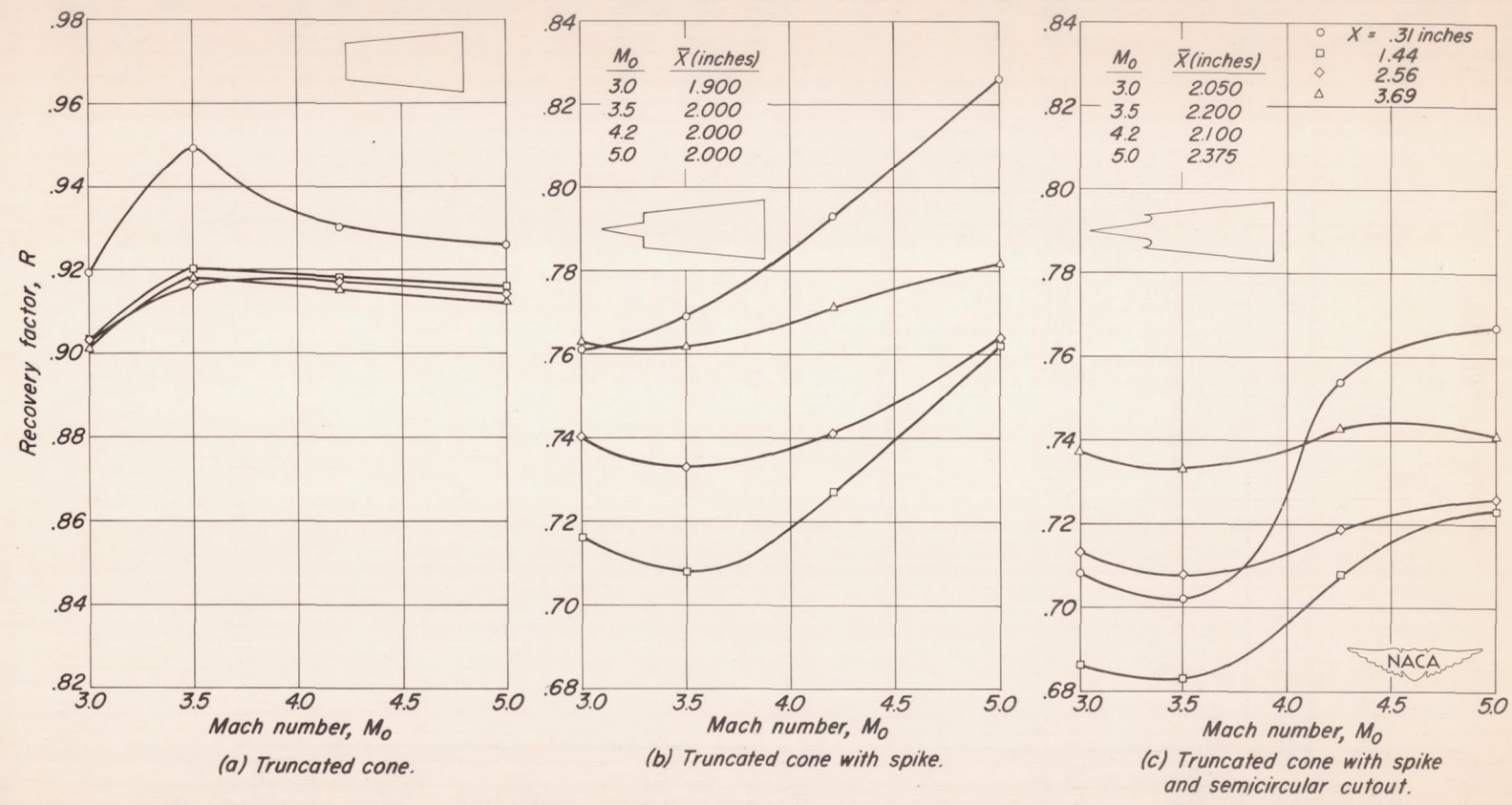
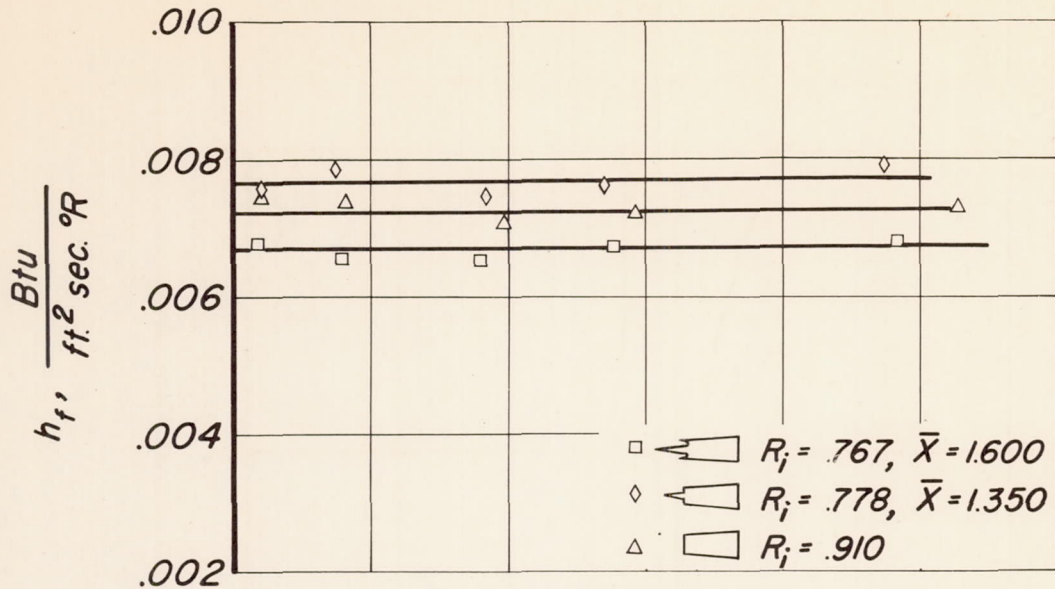
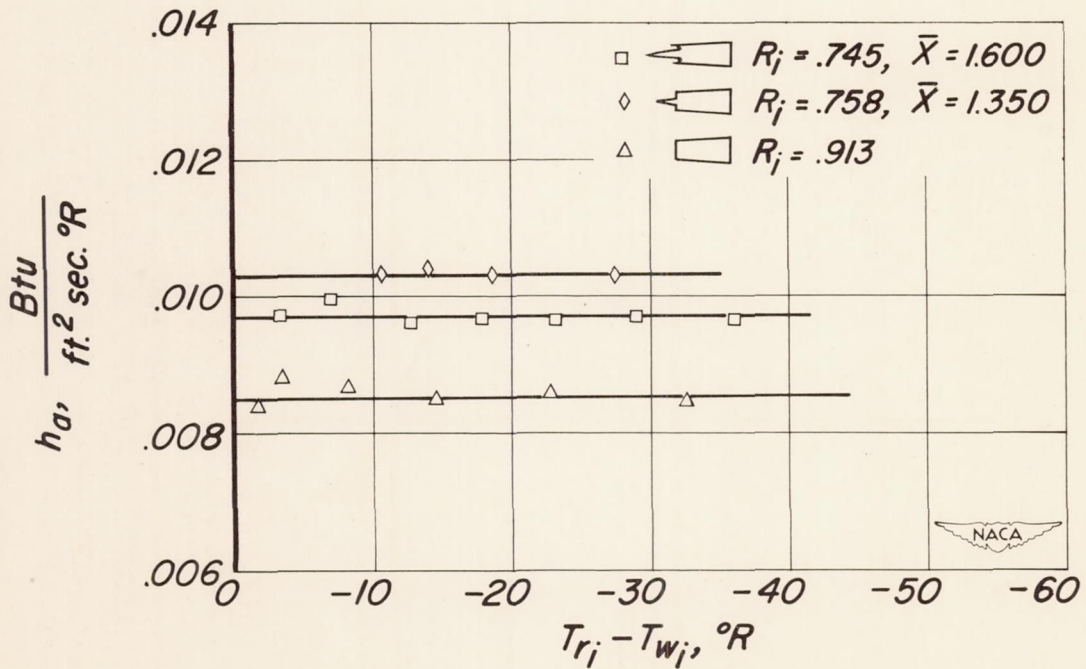


Figure 11.- Effect of Mach number on recovery factors of the different models; $\alpha = 0^\circ$.



(a) Complete models



(b) Afterbodies of models.

Figure 12.- Comparison of average heat-transfer coefficients for different body shapes; $\alpha = 0^\circ, M_0 = 3.5$.

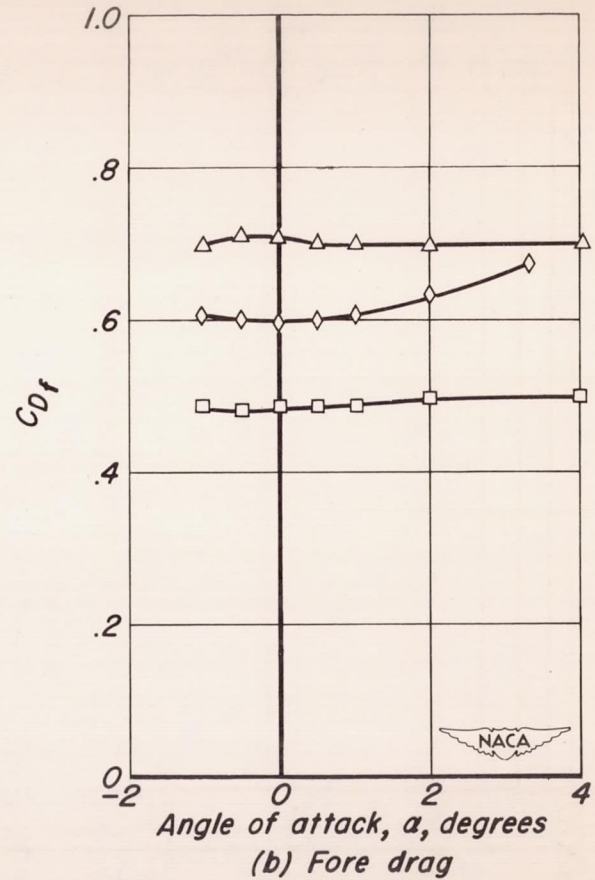
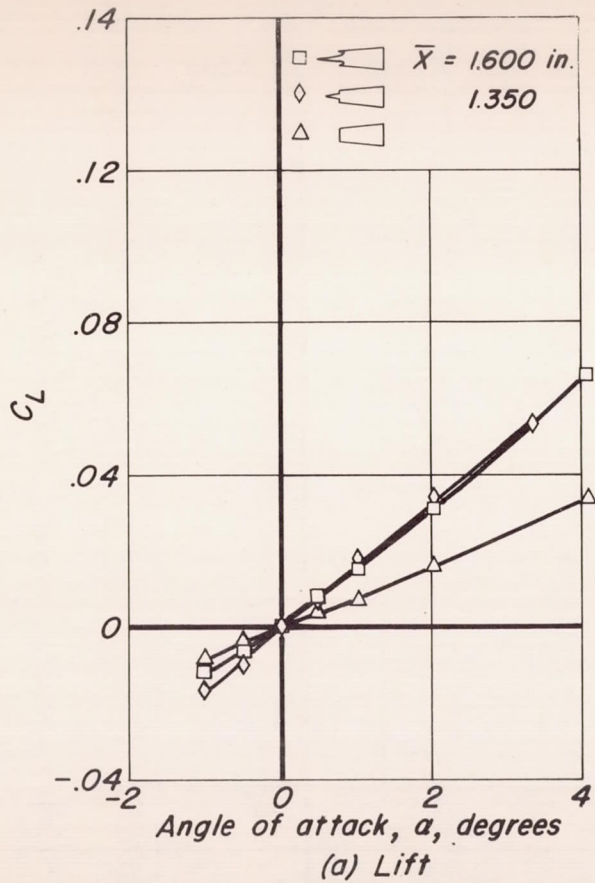
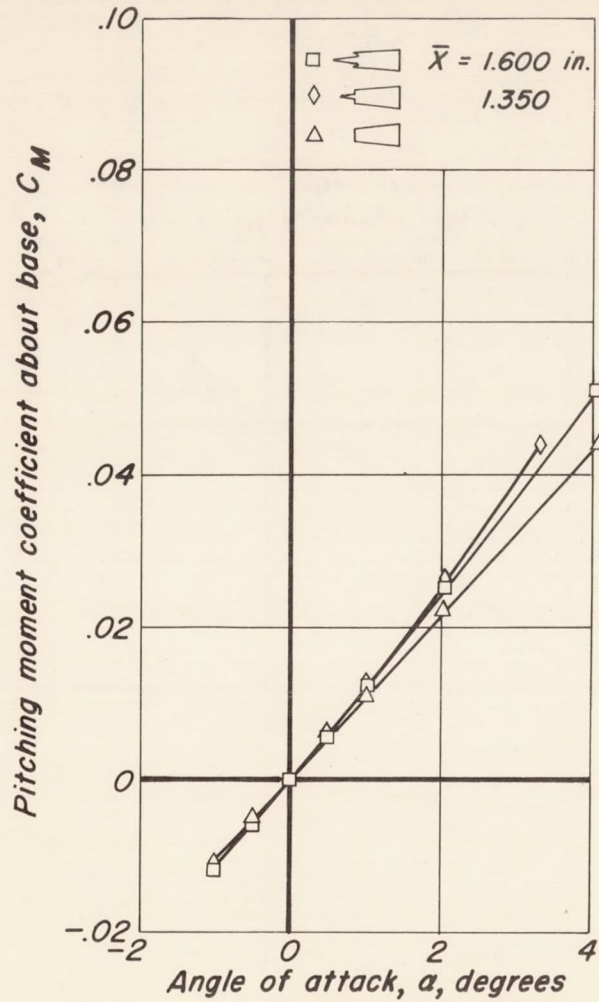
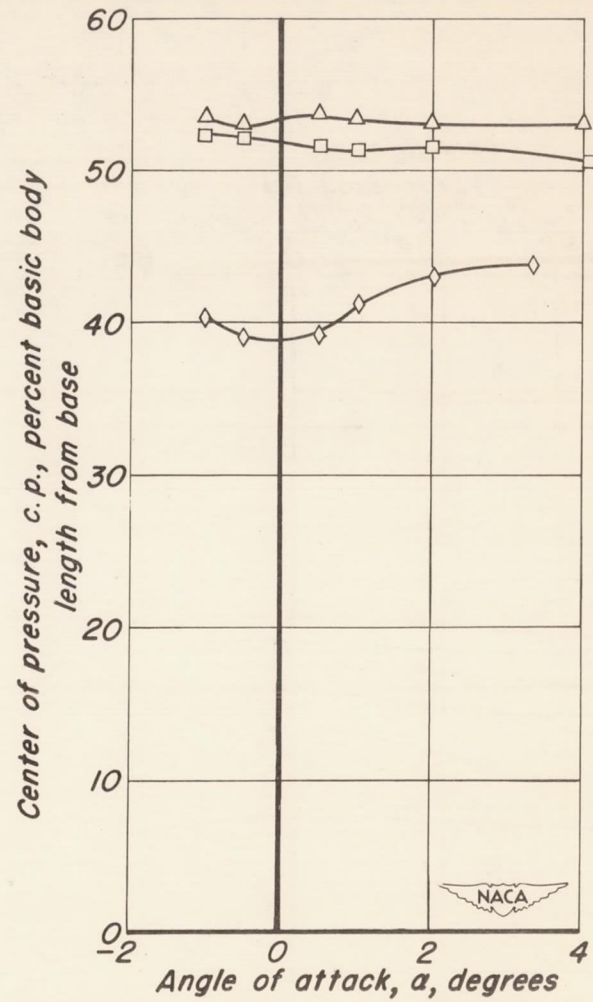


Figure 13.- Comparison of aerodynamic characteristics at angles of attack for different body shapes; $M_0 = 3.5$.



(c) Pitching moment.



(d) Center of pressure.

Figure 13.- Concluded.

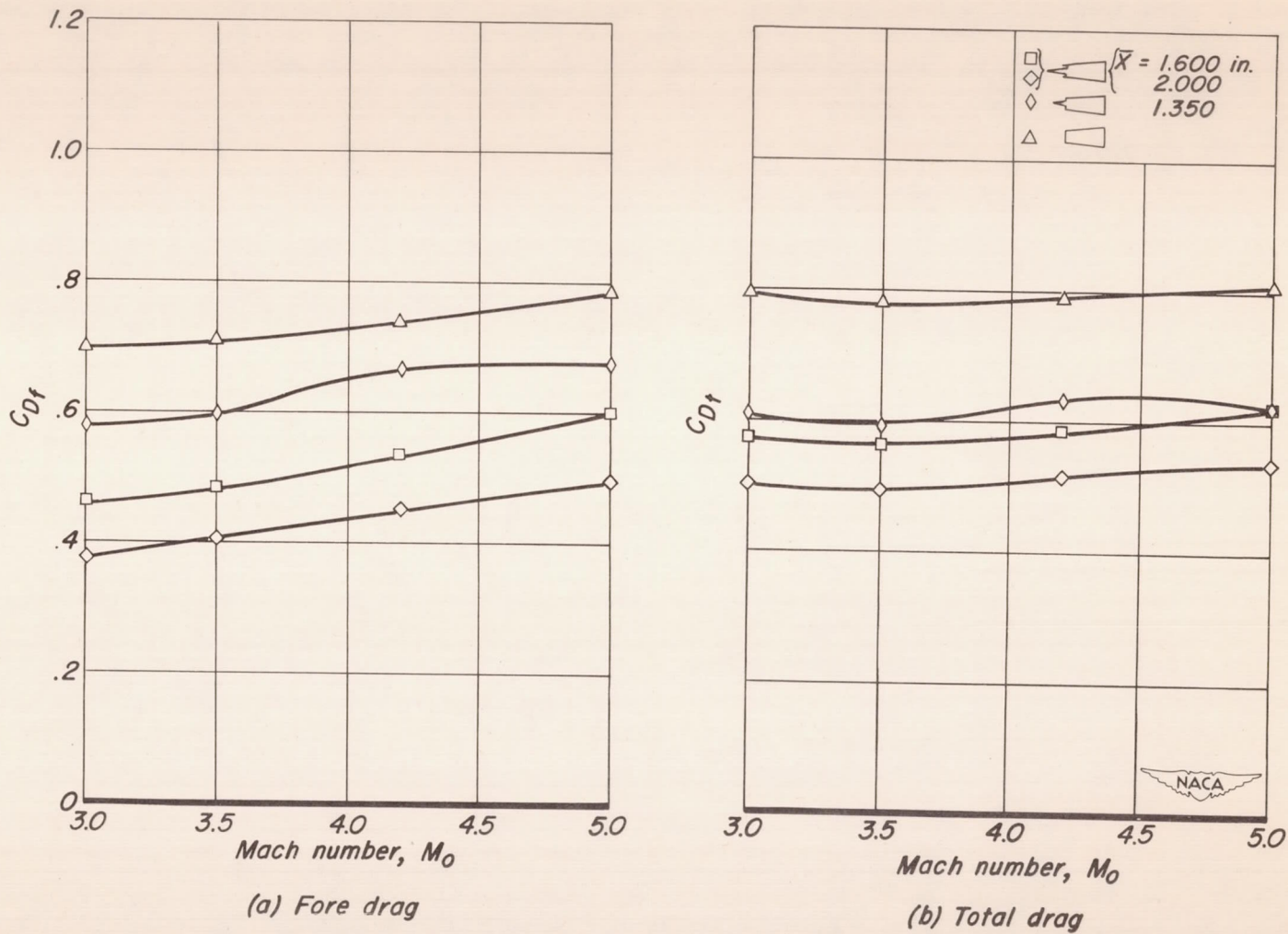


Figure 14.- Comparison of foredrag and total drag of the different model shapes at various Mach numbers; $\alpha = 0^\circ$.

CONFIDENTIAL

CONFIDENTIAL